HOST UNIVERSITY: Ghent University

FACULTY: Faculty of Engineering and Architecture

DEPARTMENT: Department of Structural Engineering and Building Materials

Academic Year 2021-2022

**Development of a Device for Small-Scale Testing of Smoke and Heat Control in Ducted Smoke Extraction Systems**

Mohammad Seyfi

Supervisors:

Prof. Bart Merci

Prof. Emmanuel Annerel

Dr. Georgios Maragkos

Master thesis submitted in the Erasmus+ Study Programme

**International Master of Science in Fire Safety Engineering**

# Disclaimer

This thesis is submitted in partial fulfillment of the requirements for the degree of The International Master of Science in Fire Safety Engineering (IMFSE). This thesis has never been submitted for any degree or examination to any other University/programme. The author declares that this thesis is original work except where stated. This declaration constitutes an assertion that full and accurate references and citations have been included for all material, directly included and indirectly contributing to the thesis. The author gives permission to make this master thesis available for consultation and to copy parts of this master thesis for personal use. In the case of any other use, the limitations of the copyright have to be respected, in particular with regard to the obligation to state expressly the source when quoting results from this master thesis. The thesis supervisor must be informed when data or results are used.

Mohammad Seyfi

10-05-2022

# Abstract

A method is proposed for small-scale testing with fire-induced smoke and heat in building compartments. In order to replicate the ceiling jet from the fire, an analogy is drawn between the purely buoyant smoke plume and a combined buoyancy and momentum-driven flow, i.e., hot air with an initial velocity. The analogy is based on preserving the momentum and energy of the actual smoke plume and translating these quantities into a uniform temperature and velocity for the flow of hot air. Estimation of the momentum and energy is based on empirical correlations for the smoke plume and integration of the Gaussian temperature and velocity profiles. The effect of plume diameter in integration is examined by comparing ceiling jets from full-scale FDS simulations with different diameters against the ceiling jets from simulations of $1\,MW$ to $3\,MW$ fires. Next, simulations with the hot air model and actual fires are downscaled with three scale factors of 1/10, 1/15, and 1/20, and a comparison of ceiling jet characteristics is made between both cases against full-scale fire simulations. The input parameters including the inlet temperature and velocity, the cross-section area, and the height of injecting hot air into the compartment are based on Froude scaling. Small-scale experiments with similar configurations using the proposed method are used to validate the simulation results by means of comparing temperature measurements. Experimental and simulation measurements of ceiling jet temperatures using the proposed method are in acceptable agreement with respect to existing empirical correlations derived from full-scale experiments. Based on the present outcomes, the proposed method can partially eliminate the discrepancies in the ceiling jet temperatures due to the weak turbulence in small-scale building spaces. However, this method is applicable for studies where the ceiling jet and smoke behavior at further distances from the fire source are more relevant than flames and smoke plume.

# Abstract in Persian (چکیده)

هدف این پایان‌نامه ارایه روشی  برای ارزیابی دود و حرارت حاصل از حریق در فضاهای ساختمانی است. به‌همین منظور، تشابهی بین ستون دود با نیروی بویانسی (شناوری) خالص و یک جریان حاصل از ترکیب نیروی بویانسی و مومنتوم، یا به بیان دیگر جریان هوای گرم با سرعت اولیه مشخص، طراحی شده است تا بتوان رفتار دود ناشی از حریق واقعی در زیر سقف را بازسازی کرد. در طراحی این تشابه، حفظ مومنتوم و انرژی ستون دود و استفاده از آن برای تعریف دما و سرعتی یکنواخت برای جریان هوای گرم مورد توجه قرار گرفته است. مومنتوم و انرژی با استفاده از روابط تجربی موجود برای ستون دود و انتگرال‌گیری از معادلات گاوسی دما و سرعت محاسبه می‌شود. اثر قطر ستون دود بر انتگرال از طریق مقایسه رفتار دود زیر سقف با استفاده از شبیه‌سازی‌های دینامیک سیالات محاسباتی FDS در مقیاس کامل و قطرهای مختلف با رفتار دود زیر سقف در مورد حریق‌هایی با اندازه‌های ۱ تا ۳ مگاوات بررسی می‌شود. سپس، مقایسه‌ای در سه مقیاس ۱/۱۰، ۱/۱۵، و ۱/۲۰ بین رفتار دود زیر سقف در شبیه‌سازی‌های مقیاس کوچک بین مدل هوای گرم و مدل حریق واقعی انجام می‌شود. در این روش مقادیر دما، سرعت، مساحت سطح و ارتفاع تزریق هوای گرم در فضا براساس روش مقیاس‌سازی فِرود (Froude) محاسبه می‌شود. به منظور صحت‌سنجی نتایج شبیه‌سازی از آزمایش‌های تجربی در مقیاس کوچک با همان مشخصات و مقایسه دمای زیر سقف استفاده شده است.  مقادیر حاصل از نتایج تجربی و شبیه‌سازی بدست آمده برای دماهای دود زیر سقف بر اساس روش پیشنهادی نسبت به روابط تجربی موجود حاصل از آزمایش‌های تجربی در مقیاس کامل از دقت قابل قبولی برخوردار است. این مطالعه نشان می‌دهد روش پیشنهادی می‌تواند تا حدی انحراف نتایج در مقیاس‌های بسیار کوچک فضاهای ساختمانی، ناشی از توربولانس ضعیف را جبران کند. لازم به ذکر است، این روش در مطالعاتی قابل اجرا است که رفتار دود زیر سقف در فاصله‌های دور از حریق نسبت به شعله حریق و ستون دود از اهمیت بیشتری برخوردار باشد.

# Table of Content

# Nomenclature

| Parameters | | Subscripts | |
|---|---|---|---|
| $H$ | ceiling height | $a$ | hot air |
| $l$ | characteristic length | $ave$ | integrated average |
| $\dot{m}$ | mass flowrate | $c$ | convective |
| $\dot{Q}$ | heat release rate | $FS$ | full scale |
| $r$ | distance from plume centerline | $p$ | smoke plume |
| $R$ | plume radius | $SS$ | small scale |
| $T$ | temperature | $0$ | plume centerline |
| $u$ | velocity | $\infty$ | ambient |
| $vr$ | velocity ratio | | |
| $z$ | height | | |
| $z_0$ | virtual origin | | |
| $\rho$ | density | | |

# 1. Introduction & Objectives

## Introduction

Proper design of smoke and heat control systems, e.g., smoke extraction ductwork in buildings, is crucial for ensuring the safety of occupants as forensics analysis of several fire deaths has shown the significant impact of smoke inhalation on fire casualties [1]. While functional aspects of common physical mechanisms for smoke and heat control might differ with respect to the system application such as pressurization, buoyancy and airflow [2], fundamental knowledge about the characteristics of fire induced smoke, the ceiling jet and the smoke layer is the first step in order to evaluate the performance of these systems.

Experimentation is a reliable tool to characterize the fire-induced smoke, particularly in full scale studies since it has the potential of providing accurate data as the flow patterns directly correspond to what would naturally occur in reality. As an example, full-scale experiments by Traina et al. on the tenability criteria in multi-compartment residential buildings, showed that closing doors between an under-fire and non-fire rooms has a considerable effect on the Fractional Effective Dose (FED) of temperature and CO [3].

Despite the potential accuracy of full-scale experiments, data collection and test replication are not always straightforward since these full-scale experiments not only are financially very demanding, but also might involve some risks for the experimenters, such as the case of the overpressure that nearly trapped the operator inside the room during experiments, reported by [4]. As an alternative option, Computational Fluid Dynamics (CFD) studies have become widely appreciated for analyzing various fire scenarios. For instance, regarding the overpressure inside the fire-room, Wegrzynski proposed an adaptive smoke and heat exhaust method based on CFD simulations, where the extraction capacity could be continuously modified proportional to the expansion of gases during the fire growth to maintain a constant pressure inside the enclosure [5].

Although CFD studies are significantly less expensive than full-scale experiments, the reliability of CFD solutions for practical engineering applications in compartments engages considerable levels of uncertainty.

Practical CFD simulations for engineering applications of fires inside compartments are generally conducted with a grid resolution of $10 \, cm$ or more due to the limitations in computation capacities, yet it was observed that even a $5 \, cm$ grid cannot satisfy all quality metrics in turbulent flows for some fire applications. Hopkin et al. used a statistical approach with 13 CFD cases to compare the significance of uncertainties related to the limited number of fire scenarios with the uncertainties due to the inadequacy of the CFD model. They concluded that the confidence of a CFD design solution in practical approaches (with a $10 \, cm$ grid resolution) is negatively affected by the parameter uncertainty for engineering applications, i.e., insufficient number of considered scenarios in engineering applications [6]. Therefore, a reliable and accessible tool for validation of full-scale or small-scale CFD results is very useful.

Small-scale experiments are well-suited for validation purposes. Scale modeling of building fires can serve as an economical and feasible tool for validation of numerical studies as a replacement for costly full-scale experiments. This is particularly beneficial for large scale reduction factors in terms of costs and ease of experimentation. Reducing the model scale has a great impact on the overall experimentation costs such as building the geometry, the required fuel, and flow equipment, which makes small-scale experiments suitable for validation of CFD studies for several fire safety engineering purposes. This would also reduce the computation costs of conducting small-scale CFD studies since the simulation time is decreased.

While small-scale experiments have the advantage of lower costs with respect to full-scale tests, proper scale modeling has the advantage of higher credibility when compared to CFD studies since the flow behavior naturally follows the patterns in real fires, and the results are intrinsically similar to reality when scaled up properly [7]. This could be very useful in evaluating the performance of the smoke and heat control systems, particularly by Authorities Having Jurisdiction (AHJ) or non-expert project stakeholders involved in decision-making for fire safety design, since observing smoke movement patterns is deemed more plausible than CFD reports in some cases for people without an expertise in fire safety. Hence, scale modeling techniques can also serve as a credible means for demonstration purposes.

# Experiments in Small Scales

Dimensionless scaling refers to preserving the similarity between the full-scale and small-scale models with respect to the relevant dimensionless groups (Pi groups), and it can comprise of geometric, kinematic, and dynamic similarities. In this regard, the results from a small-scale experiment can be extrapolated to the full-scale model if the dimensionless groups are equal between the two models. The relevant dimensionless groups in fire scaling are summarized in [8]. Unfortunately, preserving all dimensionless groups would be impractical for fire scaling, and some dimensionless groups are usually neglected in favor of preserving the most important dimensionless groups, a technique referred to as partial scaling [9].

For the case of fire modeling, two important dimensionless groups are Froude and Reynolds numbers, with the former representing the ratio of inertial to buoyant forces and the latter representing the inertial to viscous forces. However, there is always a conflict between preserving the Reynolds and Froude numbers for fire applications, unless the air is replaced in the scaled model with another medium to alter the kinematic viscosity of the medium or experiments take place with a different gravity [7]. Since this would be impractical for the majority of scaling applications in fire research, the Reynolds number is often ignored, but this results in negligible deviations as long as the buoyant plume is sufficiently turbulent, a method often referred to as "Froude modeling" [8].

In the Froude scaling method, the convection-driven phenomena such as the gas temperature and velocity can be reproduced with a high level of accuracy [10]. However, since it is not possible to preserve all dimensionless groups, some level of inconsistency is inevitable in small-scale fire experiments. In a study on a 1/7 scaled corridor subject to a room fire, Quintiere concluded that the radiation-driven parameters such as the surface temperature and the heat flux to the enclosure boundaries showed considerable deviations [10], yet the concept of Froude scaling is still very beneficial for several fire applications, including smoke and heat control systems.

Most small-scale fire experiments involve tunnels, atria, and carparks. Tunnels and atria have typically higher ceiling heights than building spaces and allow downscaling of the geometry to very small scales. For instance, Ingason and Li conducted experiments with different fire types and longitudinal ventilation speeds in a 1/23 scaled down model of a tunnel with two different ceiling heights [11]. Using the same set-up, they studied the effectiveness of different point extraction strategies on the fire growth in the tunnel [12]. The effect of smoke

extraction points on the smoke back-layering length was also studied by Jiang in a 1/20 scaled tunnel by altering the location of extraction points and the opening area [13]. The smoke back-layering effect has been also applied to carpark spaces. In a series of full-scale and small-scale experiments in Ghent University, temperature and velocity measurements were used to study the smoke back-layering in a carpark with unidirectional ventilation for different heat release rates [14].

Unlike scaling studies in tunnels, the major challenge for downscaled building spaces is the height of the model. The buoyant smoke plume is naturally highly turbulent for a large portion of the ceiling height in typical compartment fires [15]. The buoyant flow requires a certain length for the laminar-to-turbulent transition, and since the generation of baroclinic vortices in a buoyancy-driven flow cannot be manipulated arbitrarily when scaling [16], the limits of downscaling buoyant flows is restricted by the capability of the geometry to reproduce turbulent plumes, and it is recommended to have a plume Reynolds above 10,000 in the small-scale model [15].

The weak turbulence is known as the primary cause of discrepancies in modeling building spaces, and the minimum scale factor is strongly dependent on the ceiling height of the model. Thus, for large scale reduction factors the fire can no longer generate a sufficiently turbulent buoyant plume in the model. It is generally recommended to maintain a ceiling height of at least $30\,cm$ to ensure the weak turbulence does not have a significant impact on the results [17] (the paper reports from [18]). However, discrepancies were still found in the literature even at larger ceiling heights for small-scale building models. Arini conducted experiments on the smoke movement between adjacent compartments in a 1/8 scaled model of basements in a building, and by measuring the temperature in the fire room and adjacent rooms, reported that the low height of the ceiling and the small size of the fire led to very weak turbulent flows, generating deviations in gas temperatures near the ceiling [19]. Barsim et al. studied the gas temperature near the ceiling in a 2/27 model of an atrium with mechanical extraction on the roof based on Froude modeling [20]. They compared CFD simulations using different scale factors with their experimental data and concluded that temperatures in the far-field are unacceptably underestimated when the scaling factor falls below 1/2 [20]. Similarly, Zimny focused on measuring gas temperatures in a 1/4 scaled model of an unventilated room fire with small heat release rates and showed that although the effect of thermal inertia of boundaries is marginal for the early stages of fire (the first few minutes), the average measured temperatures were underestimated by up to 30% compared to full-scale

results [17]. Therefore, small-scale fire testing in building spaces is much more restricted than in tunnels and atria.

## Exclusion of Flames in Small-scale Experiments

Although the required distance for developing turbulent buoyant plumes is not adjustable for fires in small-scale experiments, when the experiment focuses on the smoke movement rather than the fire source itself, alternative solutions were shown applicable in replicating the same patterns of smoke flow, especially in the at further distances from the fire source. These models generally introduce a second fluid with a different density into the bulk fluid, for instance introducing helium in air or saltwater in fresh water. These techniques are obviously incapable of modeling flames and consequently some phenomena associated with the flames such as the radiation to the boundaries. Yet, they have proved to be accurate in modeling the important phenomena with respect to smoke layer height and smoke movement.

Using surrogate fluids to reproduce the fire plume was essentially developed based on the work of Morton et al. on the features of "gravitational convection" such as the case of a buoyant flow, and its similarity to the patterns created by a source of heat in a gas, or a source of lighter fluid in a heavier miscible fluid [21]. Steckler et al. developed the inverted saltwater technique by drawing an analogy for the equations of continuity, momentum and energy between a fire and a mixture of saltwater in fresh water. Their 1/20 scaled inverted multicompartment enclosure was filled with fresh water, and saltwater was injected with a slight initial momentum [15]. Vauquelin et al. proposed that the Richardson number (as a measure of density difference) is equally important as the Froude number in scaling models for the near-field, and aeraulic models such as the helium-air mixtures can preserve both factors in common fire applications [22]. He also experimentally studied the ventilation efficiency in a 1/20 tunnel, using a helium plume instead of hot smoke [23]. Zhao and Wang applied the helium plume analogy technique to a 1/26.5 scaled atrium and studied the gas temperature near the ceiling and the smoke interface height under a growing heat release rate [24].

While using surrogate fluids has shown to be reliable in small-scale experiments, conducting such experiments to study smoke and heat control performance may not be practical for engineering applications. For instance, modeling ventilation equipment is not straightforward with the saltwater technique, and the helium methodology

may not be economical for conducting several performance tests on downscaled building models with current scaling factor limits found in literature.

# Aim and Objectives

The present thesis evaluates the feasibility of replacing the smoke plume from the fire with a combined momentum and buoyancy driven plume in small scales, aiming at reproducing similar ceiling jet characteristics and smoke movement patterns in buildings. This allows for applying larger scaling factors in buildings by partially overcoming the issue of low Reynolds in the smoke plume when downscaling building spaces and experimenting with low ceiling heights. Thus, the proposed scale modeling could serve as a credible tool to study smoke movement in engineering applications.

This thesis is focused on the ceiling jet temperature as a measure to characterize the smoke movement within a compartment. The proposed methodology is evaluated experimentally in small scales and numerically using Fire Dynamics Simulator (FDS) in both full and small scales. The ceiling jet temperature is measured at different distances from the plume centerline. The fire heat release rate and the scaling factor are among the primary variables for these small-scale tests. FDS simulations were carried out in full and small scales in order to determine the input parameters for the experiments.

As the first step in evaluation of the proposed method, the geometry is rather simple to allow for better evaluation of results with respect to existing correlations. Experiments represent a large building area without any walls or obstructions in the vicinity of fire source. In addition, no smoke extraction system is present, thus the ceiling jet is formed without any external influence. The experimental data is compared against existing empirical correlations for ceiling jet temperature, such as the correlation by Heskestad and Hamada and the correlation by Alpert [25].

# 2. Methodology

The ceiling jet characteristics are more relevant than the flames and combustion chemistry when evaluating the performance of smoke and heat control designs, hence the physics is simplified in the present thesis by neglecting the fire source. A method is proposed to draw an analogy between a purely buoyant smoke plume and a flow driven by a combination of buoyancy and momentum, i.e., a flow of hot air with an initial momentum, as shown in Figure 1. The initial momentum compensates for the low Reynolds value of the purely buoyant plume in small-scale tests, consequently it can extend the limits of downscaling building spaces to some extent.

A momentum-driven turbulent flow differs from a purely buoyancy-driven turbulent flow in terms of vorticity generation. Yet, contrary to a purely buoyant flow, where the vorticity generation cannot be modified arbitrarily, it is possible to adjust the inlet velocity and radius in a momentum-driven flow to generate the desired level of turbulence [16]. Therefore, it can be possible to replicate the purely buoyant flow with a plume of hot air with an initial momentum. This chapter discusses a method proposed for determining the primary factors to ensure the momentum-driven flow can reproduce a ceiling jet similar with the one from an actual fire, although flames are disregarded and there are differences in the smoke plume and impingement region.
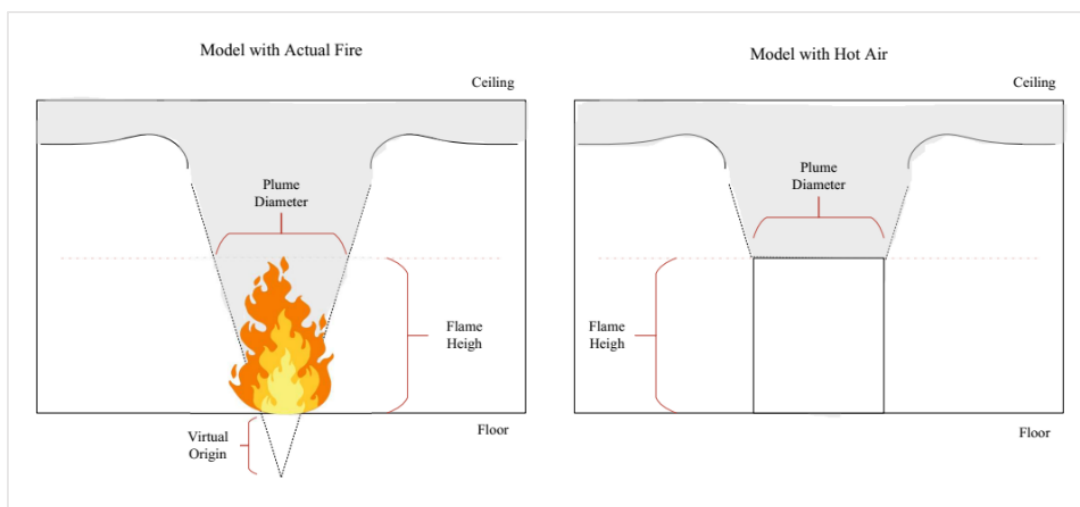


Figure 1: Analogy between the ceiling jet of an actual fire and a hot air plume with initial momentum

# Theory

In order to reproduce similar ceiling jet characteristics, primary quantities of the smoke plume must be preserved, which for the present thesis are its momentum and energy. Since the momentum and energy of the smoke plume are directly related to its temperature and upward velocity, as well as the height and diameter of the plume, the first step would be to estimate this temperature and velocity at a certain height above the mean flame height. The following section elaborates on this procedure.

Heskested plume relations have been widely used to represent the mean temperature and velocity fields in the smoke plume above the flame height [26]. These equations take the form:

$$\Delta T_0 = 9.1 \left(\frac{T_\infty}{g c_p^2 \rho_\infty^2}\right)^{1/3} \dot{Q}_c^{2/3} (z - z_0)^{-5/3} \tag{Eq. 1}$$

$$u_0 = 3.4 \left(\frac{g}{c_p \rho_\infty T_\infty}\right)^{1/3} \dot{Q}_c^{1/3} (z - z_0)^{-1/3} \tag{Eq. 2}$$

Where $\Delta T_0$ and $u_0$ represent the centerline temperature difference and velocity in the plume, respectively, $z$ and $z_0$ represent the height above the floor and the virtual origin height, $Q_c$ represents the convective heat release rate and $T_\infty$ and $\rho_\infty$ denote ambient air temperature and density. Using the centerline values, the temperature difference and the velocity fields can be represented by Gaussian profiles at a radius $R$ from the plume centerline [26], given by:

$$\Delta T = \Delta T_0 \, exp\left[-\left(\frac{R}{\sigma_{\Delta T}}\right)^2\right] \tag{Eq. 3}$$

$$u = u_0 \, exp\left[-\left(\frac{R}{\sigma_u}\right)^2\right] \tag{Eq. 4}$$

Where $\sigma_{\Delta T}$ and $\sigma_u$ are defined in [26] as measures of plume radii. In order to estimate an average velocity and average excess temperature for the smoke plume, (Eq. 3) and (Eq. 4) are integrated in cylindrical coordinates from the plume centerline up to the distance of $R_p$.

$$\pi R_p^2 u_{ave} = \int_0^{2\pi} \int_0^{R_p} u_0 \, exp\left[-\left(\frac{r}{\sigma_u}\right)^2\right] r \, dr \, d\theta$$

$$u_{ave} = \frac{1}{R_p^2} u_0 \sigma_u^2 \left(1 - exp\left[-\left(\frac{R_p}{\sigma_u}\right)^2\right]\right) \qquad \text{(Eq. 5)}$$

$$\pi R_p^2 \, \Delta T_{ave} = \int_0^{2\pi} \int_0^{R_p} \Delta T_0 \, exp\left[-\left(\frac{r}{\sigma_{\Delta T}}\right)^2\right] r \, dr \, d\theta$$

$$\Delta T_{ave} = \frac{1}{R_p^2} \Delta T_0 \sigma_{\Delta T}^2 \left(1 - exp\left[-\left(\frac{R_p}{\sigma_{\Delta T}}\right)^2\right]\right) \qquad \text{(Eq. 6)}$$

It is evident that the average values depend on the selection of the plume radius ($R_p$). In order to provide comparisons between different heat release rates, a dimensionless parameter is used by rearranging (Eq. 4), defined as the velocity ratio ($vr$) at distance $R_p$ rather than the radius itself.

$$vr = \frac{u}{u_0} = exp\left[-\left(\frac{R}{\sigma_u}\right)^2\right] \qquad \text{(Eq. 7)}$$

Evidently, the average values strongly depend on the $vr$ parameter, as shown in Figure 2 for a sample case.
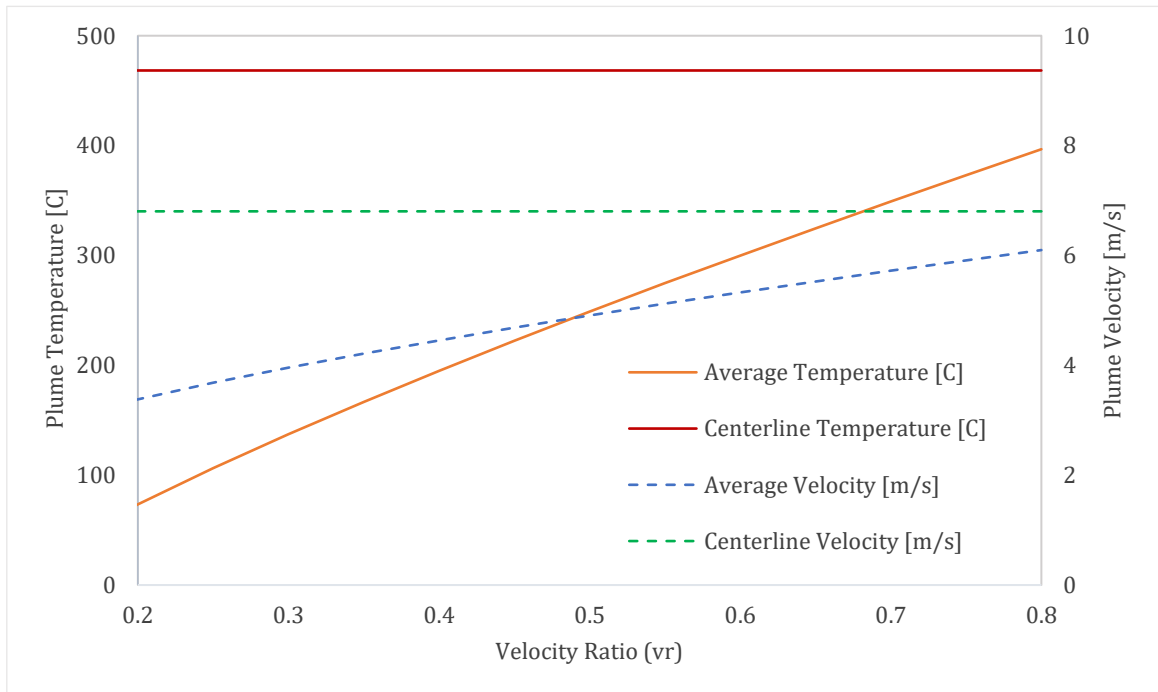


Figure 2: Effect of velocity ratio on average plume temperature and velocity
$(Q_c = 700kW, z = 1.5m, z_0 = -0.93, T_\infty = 20°C)$

In order to have a ceiling jet that follows similar characteristics of a ceiling jet formed by an actual fire, the smoke plume momentum and energy can now be calculated. These quantities can be simplified in the form of (Eq. 8) and (Eq. 9), respectively, using the integrated values and the mass flowrate of smoke plume at the same height.

$$P_b = \dot{m}_{ent} u_{ave} \tag{Eq. 8}$$

$$E_b = \dot{m}_{ent} c_p \Delta T_{ave} \tag{Eq. 9}$$

where the entrainment rate ($\dot{m}_{ent}$) can be estimated based on Heskestad's empirical relation [26], as given by:

$$\dot{m}_{ent} = 0.071 \dot{Q}_c^{1/3} (z - z_0)^{5/3} \left[ 1 + 0.027 \dot{Q}_c^{2/3} (z - z_0)^{-5/3} \right] \tag{Eq. 10}$$

Eventually, by considering the same plume diameter for the flow of hot air ($D_p = D_a$) with a uniform temperature and velocity, it is possible to specify a certain temperature ($T_a$) and velocity ($u_a$) for the jet of hot air by preserving the momentum and energy of the represented buoyancy-driven plume at a certain height $z_a$ which is at least equal to the mean flame height. This is given here by:

$$\dot{m}_{ent} u_{ave} = \dot{m}_a u_a = \rho_a \left( \frac{\pi D_a^2}{4} \right) u_a . u_a \tag{Eq. 11}$$

$$\dot{m}_{ent} c_p \Delta T_{ave} = \dot{m}_a c_p \Delta T_a = \rho_a \left( \frac{\pi D_a^2}{4} \right) u_a . c_p (T_a - T_\infty) \tag{Eq. 12}$$

Assuming a constant ambient pressure and considering the ideal gas law for the hot air, the density of hot air can be correlated to its temperature and ambient conditions through $\rho_a T_a = \rho_\infty T_\infty$, thus, (Eq. 11) and (Eq. 12) are coupled and can be solved to determine the uniform velocity and temperature that provides the equal momentum and energy in the momentum-driven flow of hot air as in the buoyancy-driven smoke plume at the specified height $z_a$.

$$\dot{m}_{ent} u_{ave} \cong \left( \frac{\pi D_a^2}{4} \right) \left( \frac{T_\infty \rho_\infty u_a^2}{T_a} \right) \tag{Eq. 13}$$

$$\dot{m}_{ent} c_p \Delta T_{ave} \cong \left( \frac{T_\infty \rho_\infty}{T_a} \right) \left( \frac{\pi D_a^2}{4} \right) u_a c_p (T_a - T_\infty) \tag{Eq. 14}$$

It should be noted that these values depend on the selection of the entrance height ($z_a$) and the diameter of the hot air flow ($D_a$). The entrance height is selected at (or slightly above) the mean flame height, and the diameter is implicitly adjusted by the previously defined velocity ratio ($vr$) throughout the present study. In principle, by selecting a design fire and calculating the mean flame height, the smoke plume is replaced with a flow of hot air at a much lower temperature while preserving the same momentum and energy contained in the plume at that height. This procedure is followed to design the input parameters for the simulations and experiments. Figure 3 illustrates important steps in calculating the uniform temperature and velocity of the hot air plume with this procedure.
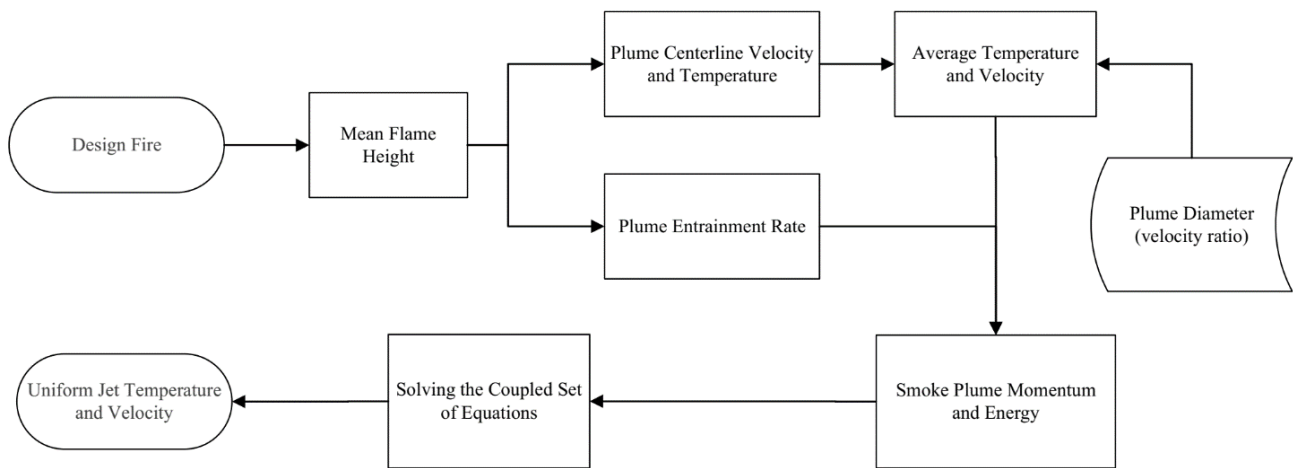


Figure 3: Calculation procedure for the uniform temperature and velocity of hot air plume

Note that uniform temperature and velocity fields were preferred for the momentum-driven flow considering the practicality of conducting experiments, as injecting the hot air with a uniform profile is easier than controlling the velocity and temperature profiles during tests. Moreover, it is evident that a longer distance from the entrance height of the hot air plume to the ceiling allows for better development of the velocity field, but this height cannot fall below the mean flame height since some of the considered correlations would no longer be valid in the flame region. Therefore, the mean flame height was selected as the lowest possible height of hot air entrance into the test section. Recalling that the average velocity and temperature from (Eq. 5) and (Eq. 6) depend on the selection of the plume diameter while the entrainment rate from (Eq. 10) is independent of this selection, no analytical connection could be made to the plume diameter in order to decide its optimum value.

Hence, different FDS cases were modeled to compare the ceiling jet characteristics between the hot air plumes with different $vr$ values and the corresponding ceiling jet from an actual fire.

# Froude Scaling

For well-ventilated compartment fires, a properly downscaled model has the same Froude number while being sufficiently turbulent (generally with Reynolds above 10,000), and there is a geometrical similarity between the model and the full-scale compartment [27]. Noting that the aim of the present thesis is primarily to study the formation of the ceiling jet, some of the important fire phenomena such as heat transfer within solid boundaries are less relevant. This is due to the fact that such phenomena would require a significantly longer time to create an impact on the formation of smoke layer [27], while the present experiments aim at studying the formation of the unhindered ceiling jet during a short period (generally a few minutes). Froude scaling starts by the geometric scale factor and the definition of Froude number in fire modeling, given by:

$$Fr = u_0/\sqrt{gl} \tag{Eq. 15}$$

Where $u_0$ and $l$ represent the velocity and the characteristic length. By considering the geometric analogy (with the geometric scale factor defined as $l_{SS}/l_{FS}$, where subscripts $FS$ and $SS$ refer to full-scale and small-scale models, respectively) the velocity can be determined as $u_{SS}/u_{FS} = (l_{SS}/l_{FS})^{1/2}$. Following the similar procedure, the scale factors can be determined for other properties, summarized in Table 1 for the relevant properties here. The present experiments and small-scale simulations were designed based on these values, and the reader is referred to [8] for a through discussion on how to obtain these factors.

Table 1: Relevant scale factors in Froude modeling for the present study

| Property | Scale Factor | Property | Scale Factor |
|---|---|---|---|
| Length | $(l_{SS}/l_{FS})$ | Velocity | $(l_{SS}/l_{FS})^{1/2}$ |
| Time | $(l_{SS}/l_{FS})^{1/2}$ | Area | $(l_{SS}/l_{FS})^2$ |
| Volume | $(l_{SS}/l_{FS})^3$ | Density | 1 |
| Heat Release Rate | $(l_{SS}/l_{FS})^{5/2}$ | Volumetric Flowrate | $(l_{SS}/l_{FS})^{5/2}$ |
| Temperature | 1 | Pressure | $(l_{SS}/l_{FS})$ |

# CFD Modeling

The first set of FDS simulations aimed at distinguishing the differences between hot air plumes with different diameters in terms of the ceiling jet characteristics. Different cases where initially modeled with $vr$ values from 0.05 to 0.5 and the results were compared with the FDS simulations incorporating an actual fire with the respective heat release rate. Based on the preliminary evaluations, 20 full-scale simulations were conducted in 5 heat release rates and 4 velocity ratios. The heat release rates ranged from 1 $MW$ to 3 $MW$ to represent the common values, and heat release rate per unit area was set to approximately $260 kW/m^2$ in reference to [28] for common office fires. The hot air plume entrance was placed close to the mean flame height to provide the maximum distance from the ceiling for the development of the flow field, although even the full ceiling height was not sufficient to fully cover the initial development region according to [29].

Based on the results of full-scale simulations, a single velocity ratio was then selected for small-scale simulations in order to evaluate the feasibility of downscaling the model with large scale reduction factors while reproducing similar ceiling jet characteristics with respect to the full-scale simulations. This comprised of 15 small-scale simulations, carried out with 5 levels of heat release rates as indicated above and 3 scale factors.

## *FDS Case Set-up*

Table 2 summarizes the main input factors in full-scale FDS simulations corresponding to different heat release rates. Note that the radiative fraction was assumed to be 30% for all simulations in the present study considering the fuel type (propane) for experiments. It should be noted that the diameter was replaced with a proportional rectangular dimension for simulations using the same cross-section area. Moreover, the temperature and velocity of the hot air flow slightly differ from the exact calculation of the previously mentioned equations since the circular jet was modeled as a square, and the rectangular cross-section area was slightly different from the original circular cross-section for some cases in order to comply with the grid size for FDS simulations. In any case, the temperature and velocity of the hot air plume correspond to the final cross-section area of the flow as implemented in FDS.

Table 2: Design inputs for full-scale FDS simulations

| Simulation ID | Fire Characteristics | | | Hot Air Plume Characteristics | | | | |
|---|---|---|---|---|---|---|---|---|
| | $HRR$ | $HRRPUA$ | flame height $L_f$ | inlet height $z_a$ | duct dimension $a_a$ | temperature $T_a$ | velocity $u_a$ | velocity ratio $vr$ |
| (F: full scale) | $[MW]$ | $[kW/m^2]$ | $[m]$ | $[m]$ | $[m]$ | $[C]$ | $[m/s]$ | - |
| F-1 | | | | | 1.65 | 143.7 | 2.18 | 0.10 |
| F-2 | | | | | 1.50 | 172.9 | 2.65 | 0.15 |
| F-3 | 1.0 | 263 | 1.48 | 1.5 | 1.40 | 200.0 | 3.08 | 0.20 |
| F-4 | | | | | 1.30 | 231.2 | 3.57 | 0.25 |
| F-5 | | | | | 1.95 | 142.9 | 2.35 | 0.10 |
| F-6 | | | | | 1.75 | 174.3 | 2.90 | 0.15 |
| F-7 | 1.5 | 262 | 1.63 | 1.65 | 1.60 | 206.4 | 3.46 | 0.20 |
| F-8 | | | | | 1.50 | 236.3 | 3.97 | 0.25 |
| F-9 | | | | | 2.15 | 146.7 | 2.53 | 0.10 |
| F-10 | | | | | 1.95 | 177.2 | 3.10 | 0.15 |
| F-11 | 2.0 | 265 | 1.75 | 1.75 | 1.80 | 207.7 | 3.65 | 0.20 |
| F-12 | | | | | 1.70 | 235.8 | 4.15 | 0.25 |
| F-13 | | | | | 2.35 | 146.8 | 2.65 | 0.10 |
| F-14 | | | | | 2.15 | 175.6 | 3.20 | 0.15 |
| F-15 | 2.5 | 260 | 1.8 | 1.8 | 2.00 | 204.1 | 3.74 | 0.20 |
| F-16 | | | | | 1.85 | 237.2 | 4.36 | 0.25 |
| F-17 | | | | | 2.55 | 145.5 | 2.72 | 0.10 |
| F-18 | | | | | 2.30 | 176.7 | 3.35 | 0.15 |
| F-19 | 3.0 | 265 | 1.9 | 1.9 | 2.15 | 204.2 | 3.88 | 0.20 |
| F-20 | | | | | 1.95 | 242.9 | 4.64 | 0.25 |

## Mesh Sensitivity Analysis

The characteristic fire diameter [30] was calculated for the smallest fire size in Table 2 as $D^* = 0.96\ m$, and using this value as the first estimate, $10\ cm$ cell size was refined to $5\ cm$, and $2.5\ cm$ for the mesh sensitivity analysis, showing that a grid size of $5\ cm$ is sufficient for the present simulations. Figure 4 compares the temperature measurements for these cases at a distance of $5\ m$ from the plume centerline. In addition, the viscous wall units ($y^+$) were found to be within an acceptable range at the ceiling boundary for $5\ cm$ cells (being below 300 similar to [6]). The level of accuracy is considered acceptable in modeling the near-wall turbulence when $y^+$ is generally $\mathcal{O}(100)$ according to the FDS User Guide [30].
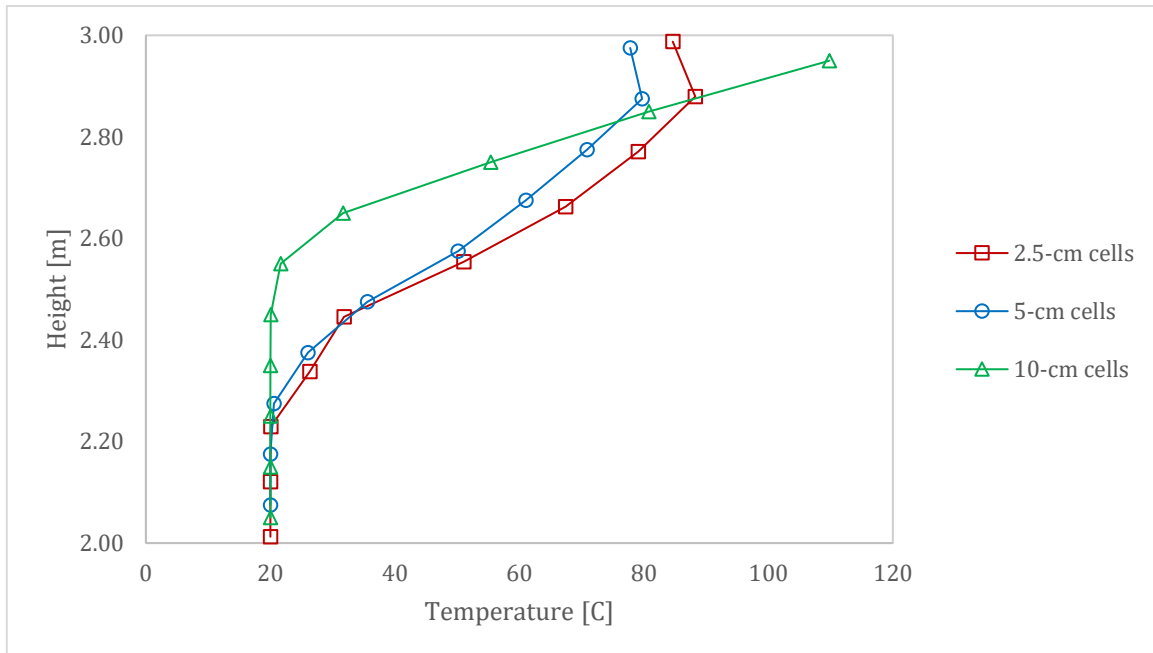


Figure 4: Mesh sensitivity analysis for full scale simulations

### Computation Domain and Boundary Conditions

The domain was $12\ m$ long and $8\ m$ wide with a ceiling height of $3\ m$ and the plume located in the center. The boundaries on the sides were open. Although heat conduction through the ceiling is less relevant for such short duration of simulations, thermophysical properties of concrete were selected for the ceiling. For the cases with an actual fire, the burner was placed on the floor level, and for the cases with the hot air plume, a vent was placed inside a rectangular duct with a specified temperature and velocity. The rectangular duct modeled the entrance duct built for experiments, and adiabatic boundary conditions were assigned to its surfaces.

## Physical & Numerical Modeling

It was seen that steady-state conditions appear after $30\ s$, thus simulations were carried out for a duration of $60\ s$, and the measurement values were averaged over the last $20\ s$ (similar to [31]). Moreover, in the absence of a fire source, the maximum temperature is approximately $243\ ℃$ as presented in Table 2, which indicates that a negligible portion of the total heat transfer takes place by radiation. Assuming the maximum radiative heat transfer between objects with the highest and lowest temperatures of $250\ ℃$ and $20\ ℃$, the net radiative heat transfer was in the order of a few kilowatts, being negligible compared to the total heat release rates for these simulations. Therefore, the radiation solver was turned off for these simulations to save the computation time. For the simulations with actual fires, the radiative fraction was set to 30% corresponding to the fuel type.

## Measurement Devices

The primary measurements for the present study were related to the ceiling jet temperature and horizontal velocity, thus these measurement devices are placed along the $z$ axis in the positive $x$ direction ($y = 0$) at different distances from the plume centerline with an interval of $0.5\ m$, as shown in Figure 5.
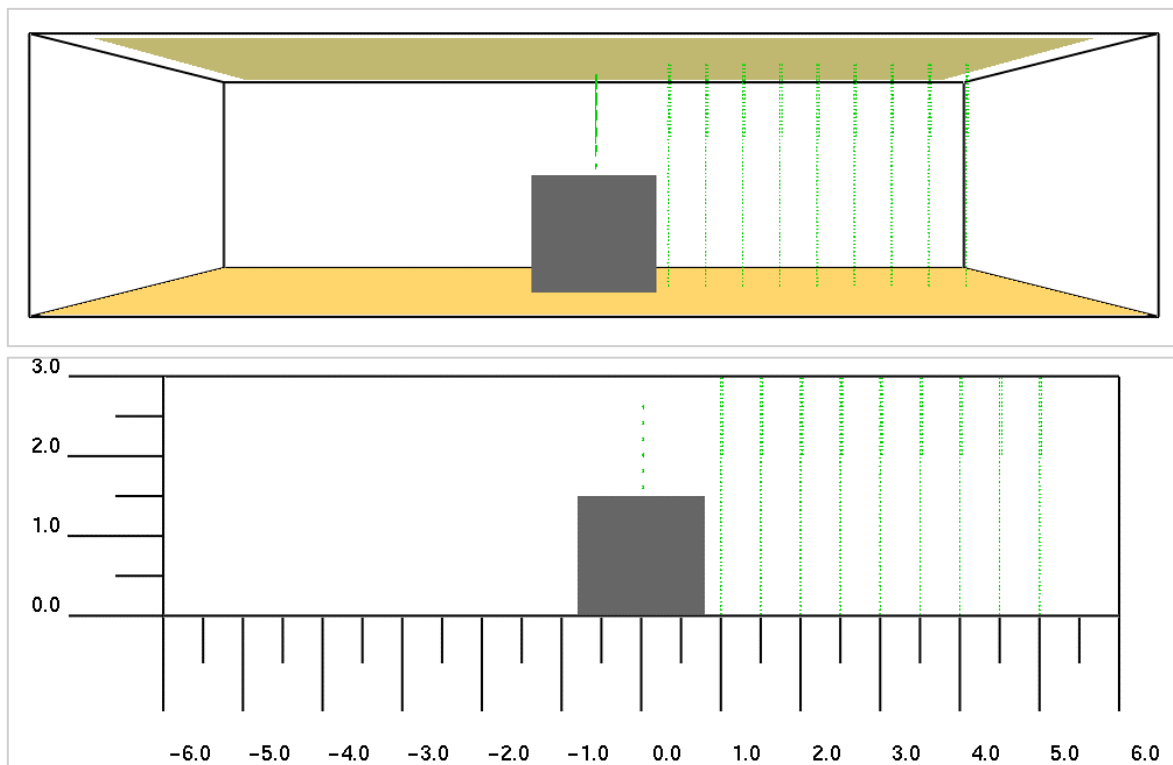


Figure 5: Computation domain and measurement devices in full-scale simulations

## Small-scale Simulations

The computation domain was scaled down with three different geometric scale factors, while the number of the cells in each direction was equal to the full-scale model. The other parameters including the heat release rate, the cross-section area and velocity were downscaled according to Table 1. In total, 15 CFD simulation were carried out with three geometric scale factors of 1/10, 1/15, and 1/20. The corresponding inputs for small-scale simulations set-up are summarized in Table 3.

Table 3: Design inputs for small-scale FDS simulations

| Simulation ID | Corresponding Full-scale Simulation | Scale Factor | Small-scale Hot Air Plume Characteristics | | | | |
| | | | $HRR$ | inlet height $z_a$ | duct dimension $a_a$ | temperature $T_a$ | velocity $u_a$ |
| (S: small scale) | (F: full scale) | | $[kW]$ | $[mm]$ | $[mm]$ | $[C]$ | $[m/s]$ |
| S-1 | FS-3 | 1/10 | 3.162 | 150 | 140 | 200.0 | 0.97 |
| S-2 | FS-7 | 1/10 | 4.743 | 165 | 160 | 206.4 | 1.10 |
| S-3 | FS-11 | 1/10 | 6.325 | 175 | 180 | 207.7 | 1.15 |
| S-4 | FS-15 | 1/10 | 7.906 | 180 | 200 | 204.1 | 1.18 |
| S-5 | FS-19 | 1/10 | 9.487 | 190 | 215 | 204.2 | 1.23 |
| S-6 | FS-3 | 1/15 | 1.148 | 100 | 90 | 208.2 | 0.83 |
| S-7 | FS-7 | 1/15 | 1.721 | 110 | 110 | 199.4 | 0.86 |
| S-8 | FS-11 | 1/15 | 2.295 | 117 | 120 | 207.7 | 0.94 |
| S-9 | FS-15 | 1/15 | 2.869 | 120 | 130 | 210.0 | 1.00 |
| S-10 | FS-19 | 1/15 | 3.443 | 127 | 140 | 209.7 | 1.03 |
| S-11 | FS-3 | 1/20 | 0.559 | 75 | 70 | 200.0 | 0.69 |
| S-12 | FS-7 | 1/20 | 0.839 | 83 | 80 | 206.4 | 0.77 |
| S-13 | FS-11 | 1/20 | 1.118 | 88 | 90 | 207.7 | 0.82 |
| S-14 | FS-15 | 1/20 | 1.398 | 90 | 100 | 204.1 | 0.84 |
| S-15 | FS-19 | 1/20 | 1.677 | 95 | 105 | 209.7 | 0.89 |

The characteristic fire diameter, $D^*$ would be downscaled with the geometric scale factor since only the heat release rate is scaled with a factor of $(l_{SS}/l_{FS})^{5/2}$ while $D^*$ is proportional to $\dot{Q}^{2/5}$, hence the resultant $D^*$ would be scaled with the same geometric scale factor. A similar sensitivity analysis was conducted for a scale factor of 1/10, which led to the same conclusion of 5 $mm$ cell size. The comparison of temperature measurements is shown in Figure 6 for the three downscaled grid sizes, indicating that 5 $mm$ cells are sufficiently accurate for the present study.
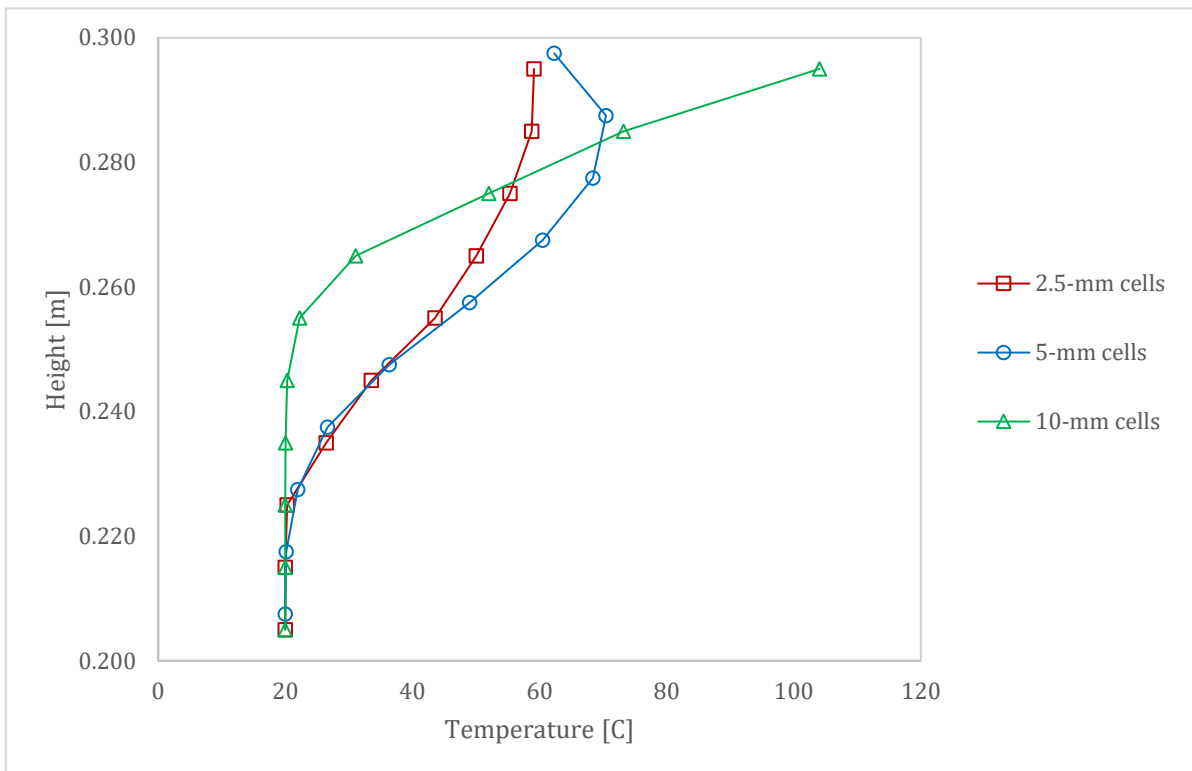


Figure 6: Mesh sensitivity analysis in small scale (scale factor of 1/10)

# Design of Experiments

This section provides a description of the experimental set-up and its components, as well as the experimentation procedure and data collection method. The experiments were designed based on the outcomes of the small-scale CFD simulations in the previous section. In order to evaluate the applicability of such method in very small scales, three scaling factors of 1/10, 1/15, and 1/20 were considered for the experiments. Since a ceiling height of $3\ m$ was assumed for the full-scale model, experiments required a ceiling height of $30\ cm$, $20\ cm$, and $15\ cm$, respectively. The heat release rates corresponded to fires of $1\ MW$ to $3\ MW$ in full scales. This range covers the typical office fires as discussed in the CFD section.

## *Overview of Experimental Set-up*

An overall view of the main equipment (E1 to E5), measurement devices (M1 to M4), and boards (B1 to B9) in the experimental set-up is illustrated in Figure 7. The aim of the present experiments was to reproduce the ceiling jet formed by the fire-induced smoke plume and measure its temperature in a scaled compartment, with the fire source replaced by a flow of hot air. For this purpose, the ambient air entered the set-up in a specified flowrate through the fan (E1) and the throttle vale (E2) and was then heated up to the specified temperature in the combustion chamber. Heat was added by means of a Meker Burner (E3), which burned propane from an external tank (E4). The flow of hot air entered the set-up using a particular ductwork that matched the required height and cross-section area according to the previously mentioned small-scale simulations. Measurements (M4) took place inside the compartment to characterize the formation of the ceiling jet with different scale factors. Since the set-up aimed at representing a large room where the ceiling jet can be formed without any external effects from nearby walls, the ceiling board was supported by four columns, and fresh air was supplied naturally into the compartment from all sides.
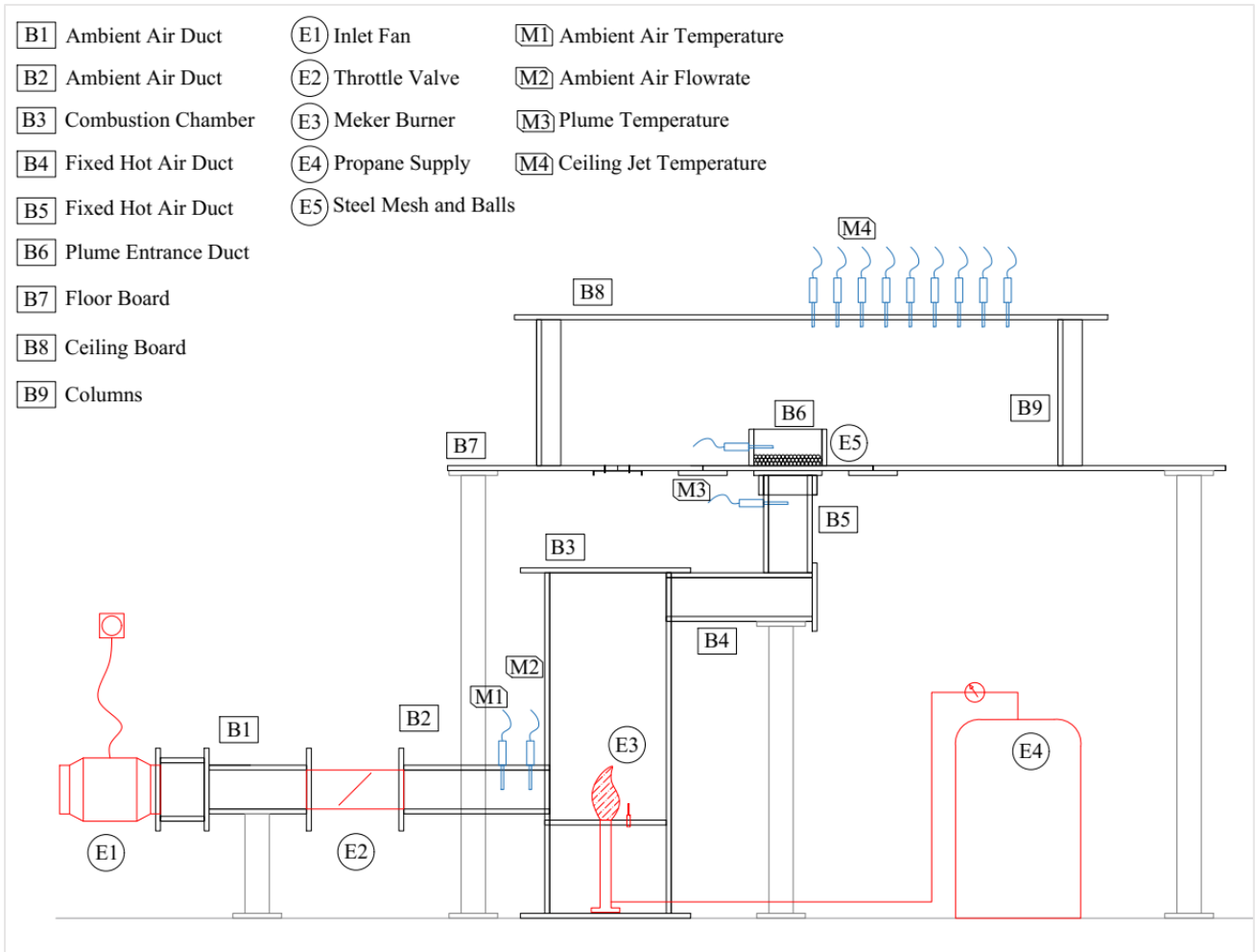
Figure 7: Overview of the experimental set-up

## Construction of Set-up

The set-up is primarily built from Promatect-H boards (shown by B1 to B9 in Figure 7). There was no need for additional insulation to the ductwork since the high thermal insulation properties of the boards would satisfy the adiabatic surface conditions described in the FDS simulation section. Important parts shown in this figure include the fixed ductwork for ambient air (B1 & B2), the combustion chamber (B3), the fixed ductwork for hot air (B4 & B5), as well as the floor (B7), the ceiling (B8), and the columns (B9) of the compartment, and eventually the interchangeable duct assembly for plume entrance (B6). The geometric scale factor was represented by the ceiling height, i.e., the height of columns (B9), and these columns for the considered scale factors are shown in Figure 8.
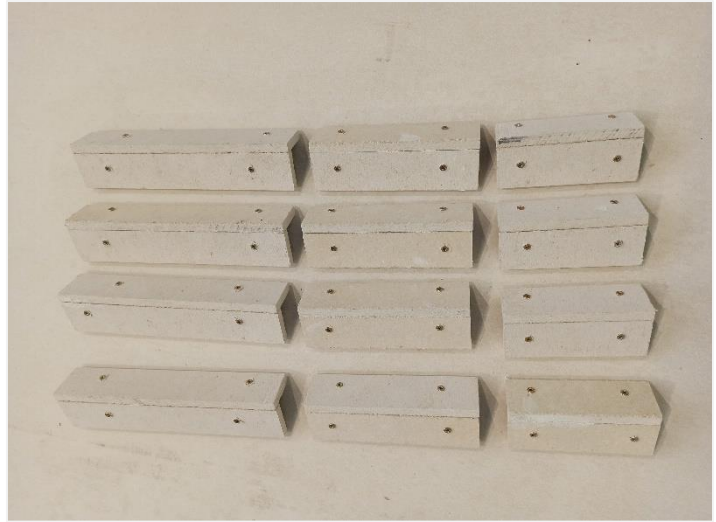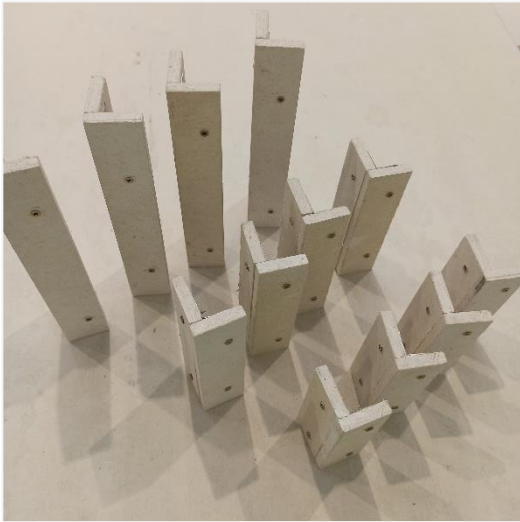
Figure 8: Columns to support the ceiling board for experiments

Aside from the columns, the interchangeable duct assembly for plume entrance (B6) was the only part that was altered for different tests. This was to facilitate the preparation of the set-up for each test according to the required height and cross-section area of the hot air plume in the compartment without the need to change the other parts for each test. This assembly is shown in Figure 9 for a sample duct. The upper part of the assembly differed according to the required height and dimensions while the size of the mounting board and the lower duct were constant.
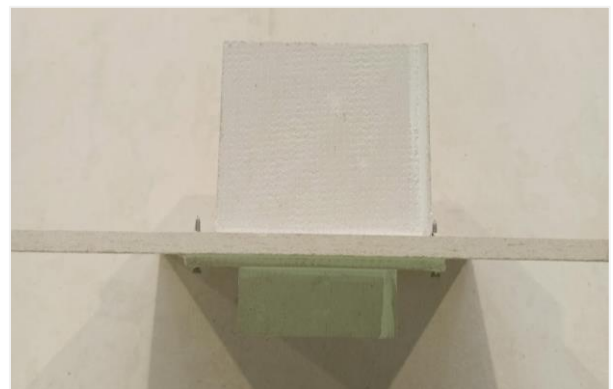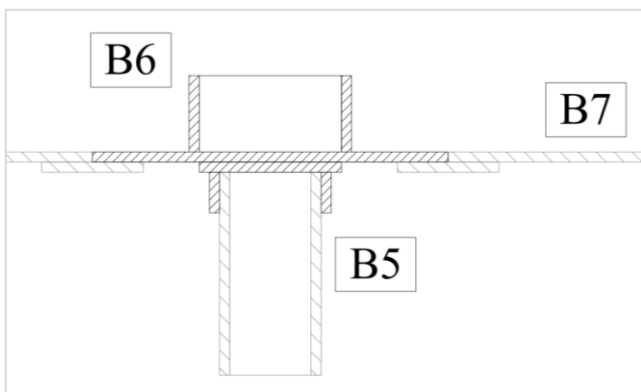


Figure 9: Interchangeable assembly for plume entrance duct

The present design facilitated the integrity of the experimental set-up since there would be fewer connection joints to be sealed for air penetration. In addition, exchanging a single part facilitated the process of preparing the set-up for each test. Some of these assemblies are shown in Figure 10.

Figure 10: Different plume entrance duct assemblies for different tests

In order to ensure the uniformity of the velocity and temperature fields at the entrance of hot air into the compartment, a steel mesh was placed inside the entrance duct to support the steel balls, as shown in Figure 11. Using steel balls was also beneficial in terms of stabilizing the temperature of the hot air plume once they reached a steady temperature since they acted as a heat reservoir and compensated for slight fluctuations of hot air temperature.



Figure 11: Steel mesh and balls to homogenize the hot air flow (E5)

## *Adjusting Input Parameters*

While the inlet height and the cross-section area of the entrance plume were adjusted by selecting the respective entrance duct assembly, the temperature and the velocity of the plume were regulated during experiments. The inlet fan (E1), shown in Figure 12, had a stepless motor connected to a potentiometer with Pulse Width Modulation (PWM) in order to continuously regulate its speed, and consequently the flowrate according to the requirements. In addition, the throttle valve (E2) shown in this figure was manually adjusted in different positions to provide additional static pressure drop, required for delivery of very low flowrates within the operating limits of the fan.



Figure 12: (top) The inlet fan with PWM regulation (E1), and (bottom) the throttle valve (E2)

It should be noted that the required volumetric flowrate of hot air plume at the target temperature was translated into the corresponding flowrate of air at ambient temperature through the ideal gas law. This is due to the fact that at the time of these experiments, no fan was found with the proper size and stepless speed regulation, and capable of continuously operating at high temperatures above 300 ℃.

The temperature of the plume was adjusted through regulation of the fuel consumption by the burner. Figure 13 illustrates the configuration and dimensions of the combustion chamber (B3) and locates the Meker Burner inside. Ambient air entered the chamber using duct B2 and the heated air left the chamber with duct B4. While the required oxygen for the premixed flame was supplied from outside the system, this value was calculated and found to be negligible with respect to the bulk flow of air, considering the high combustion efficiency of a Meker Burner and the low amount of required heat to increase the temperature of the main flow. Note that the lower part of the chamber was open to allow for free supply of fresh air. The fuel burning rate was regulated using an external valve on the propane supply line.
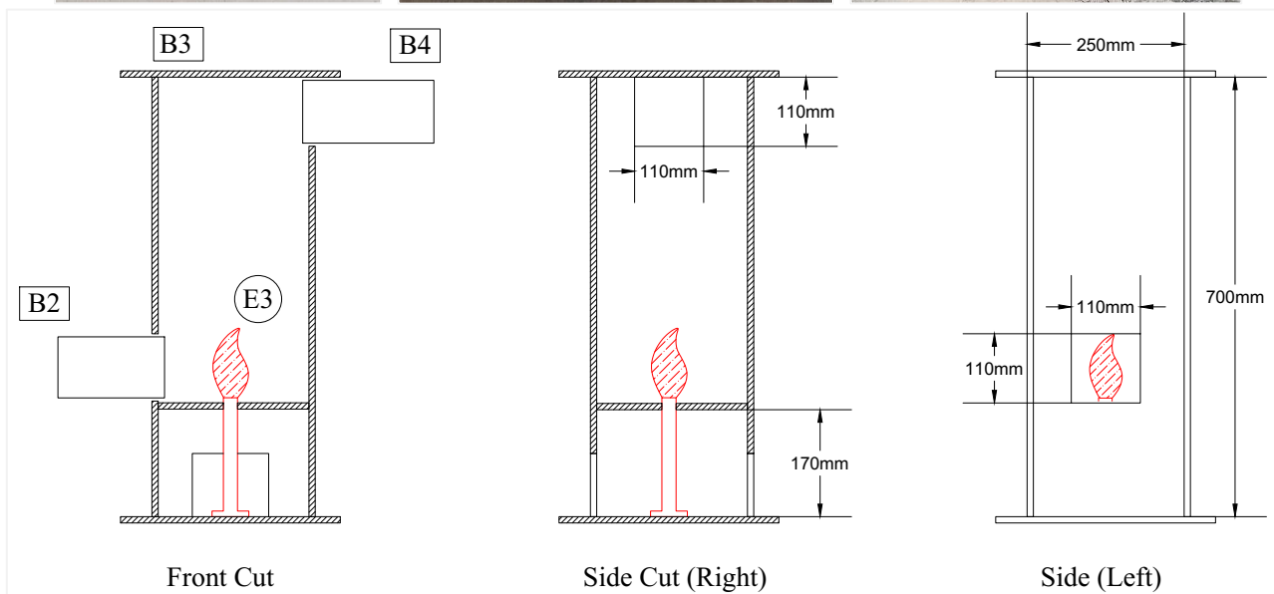


Figure 13: The Meker Burner (E3) and its location inside the combustion chamber (B3)

## Measurement Instruments

In order to correlate the ambient flowrate with the plume flowrate, thermocouples were placed in the bulk flow before entering the combustion chamber (M1) and at the plume entrance duct (M3), while the volumetric flowrate was measured using a thermal anemometer (M2), as shown in Figure 14. Inside the compartment, thermocouples were primarily placed below the ceiling at different locations from the plume centerline in order to measure the ceiling jet temperature (M4). These measurements were the key experimental data to be used for validation of simulation results, as well as being compared against existing empirical correlations based on full-scale experiments.



Figure 14: Thermal anemometer (Left) and thermocouples (Right) for flowrate and temperature measurement

## Experimental Factors and Data Collection

Since these experiments serve as the first step in evaluating the feasibility of the proposed method to model the ceiling jet in small-scale studies, the input factors were limited in order to provide the opportunity of validating the results with well-known empirical correlations. Hence, the two input parameters for experiments were the scale factor (ceiling height) and the heat release rate. Experiments followed the inputs of small-scale simulations, i.e., 3 scale factors of 1/10, 1/15, and 1/20 and 5 corresponding heat release rates of 1 $MW$ to 3 $MW$ in full scales. However, three scenarios with the largest fires in 1/10 scale were omitted due to the restrictions imposed by the operation limits of the inlet fan.

Here, the geometry represents a very wide room, for which the walls have no impact on the formation of the ceiling jet. This is ensured by a flat ceiling supported on columns at its corners, as shown in Figure 15. This configuration is well investigated in full scale [25], thus it serves as a useful point of comparison between the present model and existing empirical correlations. The fresh air can enter the test section from all directions without any obstacles.
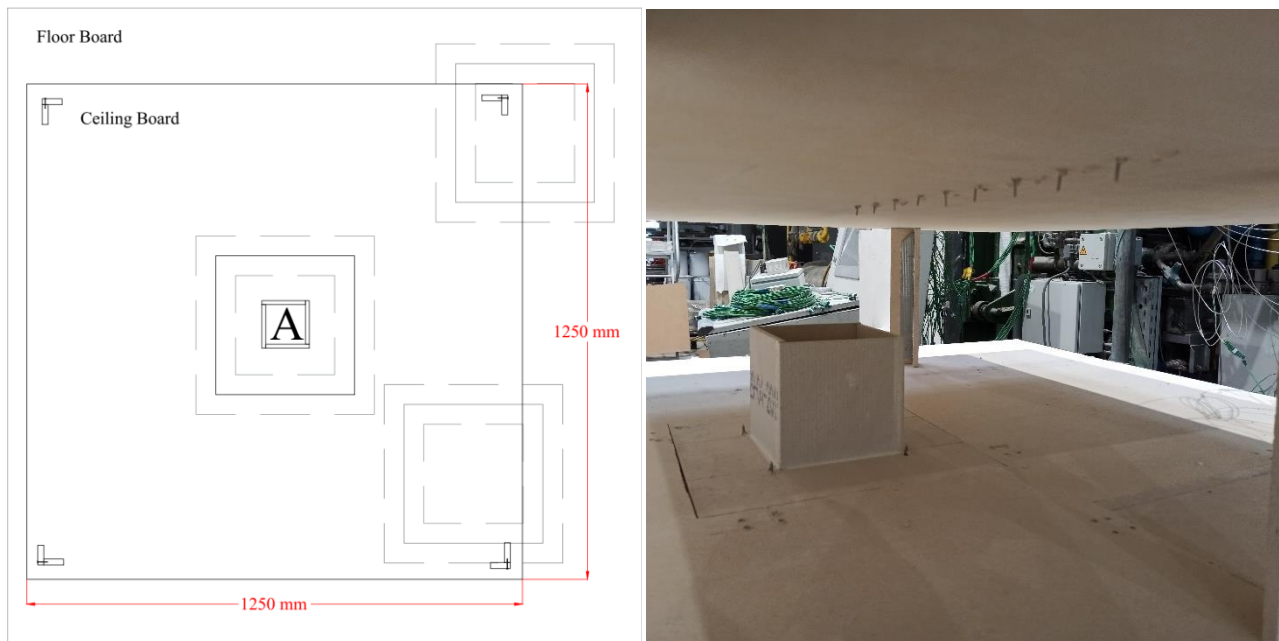


Figure 15: Location of the fire in the center of a large room

For each test, first the proper hot air entrance duct was fixed and the connection joints were sealed with aluminum tape. The distance of the first ceiling jet thermocouple was always measured from the centerline before running each test in order to monitor any displacement of the ceiling board while changing the entrance duct. Next, the ambient volumetric flowrate was adjusted according to the design inputs and then, the burner was turned on. It was seen that the combustion had a considerable impact on the delivered volumetric flowrate since the temperature rise inside the combustion chamber would impose an additional pressure drop on the fan. Since any change to the volumetric flowrate of the fan would similarly impact the temperature at the entrance duct, it was necessary to readjust the fan speed and the propane burning rate several times before reaching the target temperature and flowrate. Then, the temperature readings were monitored until the steel mesh and balls inside the entrance duct were heated up to a steady state temperature. Finally, the actual measurements were recorded for a minimum duration of 10 minutes for each test.

# 3. Results

This chapter is divided into three sections. The first section presents a comparison of full-scale FDS results using hot air plume against the FDS models incorporating an actual fire with the corresponding size. Next, a similar comparison is drawn between the full-scale and small-scale FDS results to illustrate the possibility of using such method with different scale reduction factors. Finally, the measurement data from experiments are compared against corresponding full-scale and small-scale simulations with hot air plume for validation purposes.

## Full-scale FDS Results

Temperature and horizontal velocity are measured at different distances from the plume centerline (denoted here by $x$) for all full-scale FDS simulations, as shown in Figure 16 for a sample fire size of $2\ MW$.
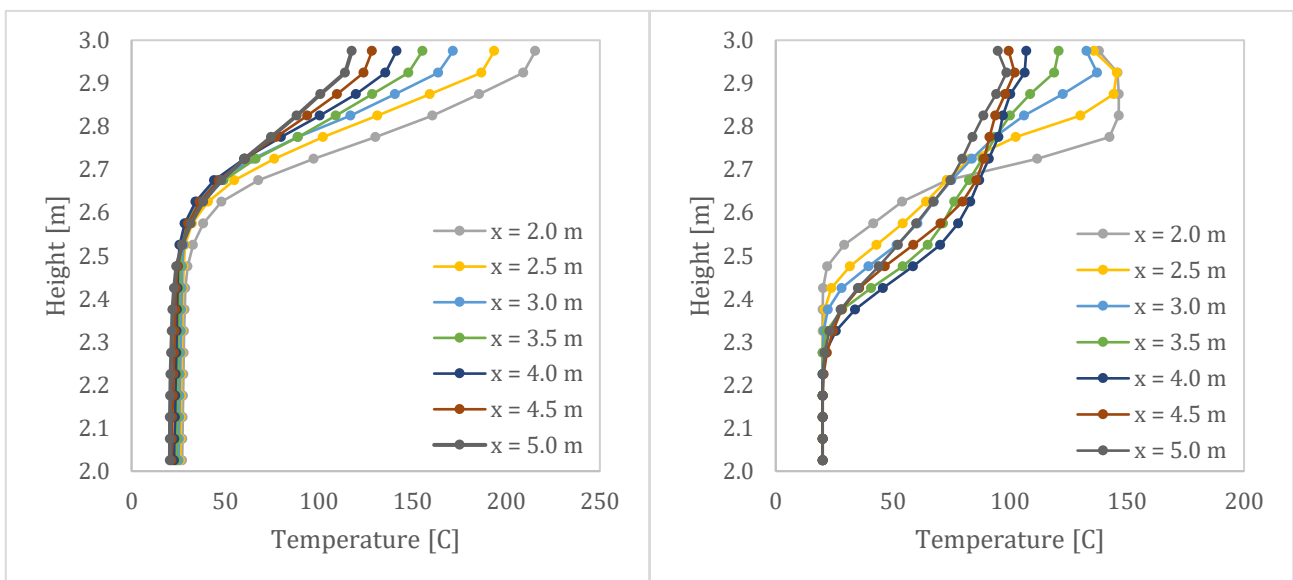


Figure 16: Temperature measurements, for (Left) actual fire and (Right) hot air model

It can be seen that temperature deviations are significant at short distances from the plume centerline. Note that the hot air injection opening was 1.1 $m$ wide for the example shown in Figure 16, thus flow patterns are expected to be naturally different from a purely buoyant flow near the plume and impingement regions. However, the present model aims at reproducing similar ceiling jet characteristics at further distances downstream.

By comparing the temperatures at distances further from the centerline, it can be seen that the maximum ceiling jet temperature is slightly lower for the proposed model, but the ceiling jet thickness is larger than the case of an actual fire. Therefore, the maximum temperature cannot solely serve as a proper representation of the ceiling jet behavior. Instead, it is more useful to compare an average temperature over the complete ceiling jet thickness. Looking at the temperature differences at different heights for the simulations including actual fires, the ceiling jet thicknesses were assumed as 25 $cm$ for 1.0 $MW$ and 1.5 $MW$ fires, and 30 $cm$ for 2.0 $MW$, 2.5 $MW$, and 3.0 $MW$ fires. This estimation follows the definition introduced by Alpert for the height where the excess temperature falls below $e^{-1}$ times of its maximum value [25]. Similar averaging thicknesses were considered for the FDS cases corresponding to each fire size.

Using the similar thicknesses and the measurements for the ceiling jet horizontal velocity, the volumetric flowrate of the ceiling jet can be estimated at each distance as $2\pi\, r\, u\, z$, where $r$ represents the distance from the plume centerline while $u$ and $z$ represent the horizontal outward velocity and the simulation cell size, respectively.

Figure 17 and Figure 18 illustrate the average velocity and volumetric flowrate at different distances from the plume centerline and draw comparisons between FDS cases with hot air plume and the corresponding FDS cases with an actual fire. Note that the difference between the models lies in the selection of the velocity ratio ($vr$), which is inversely related to the cross-section area of the hot air entrance duct.
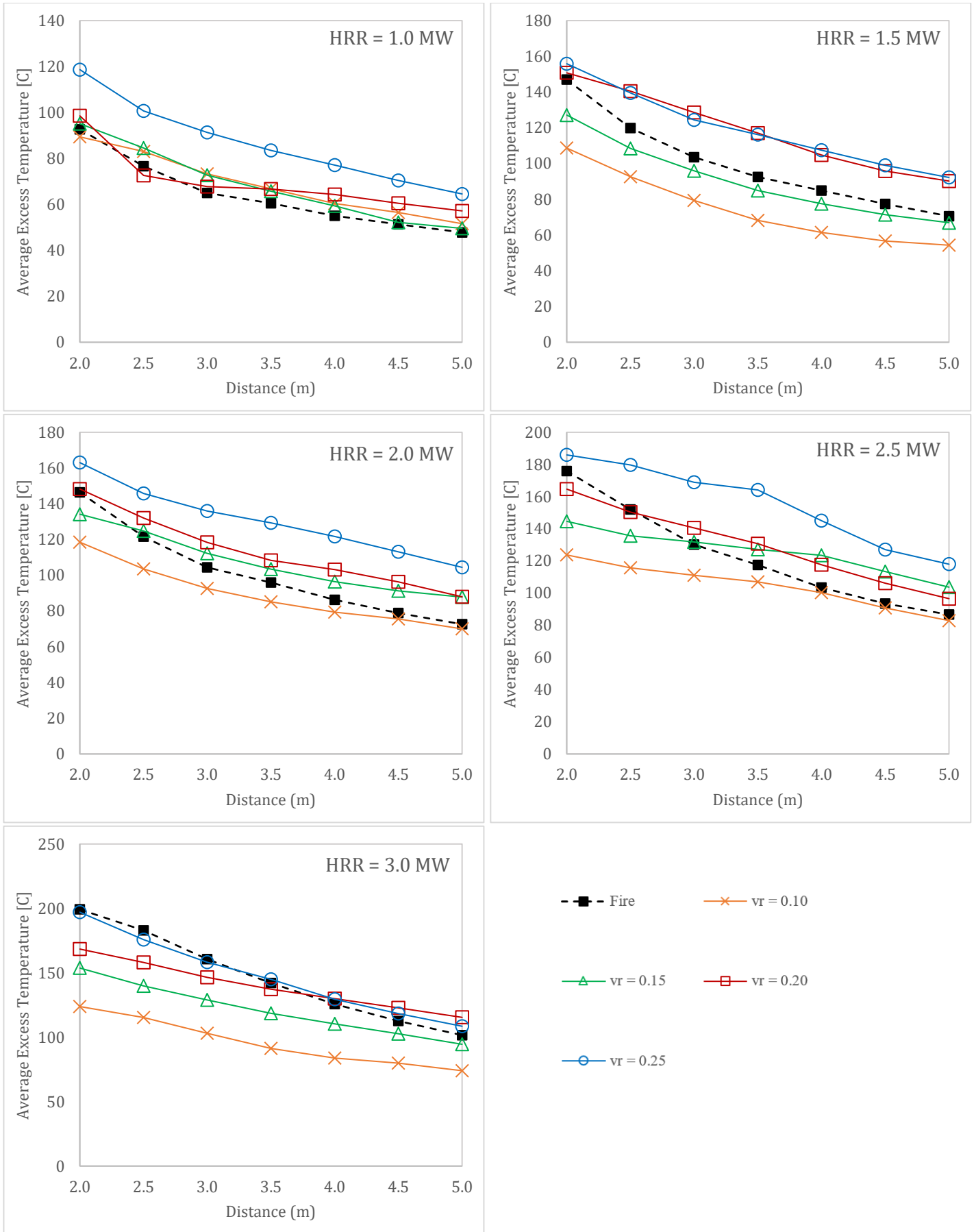
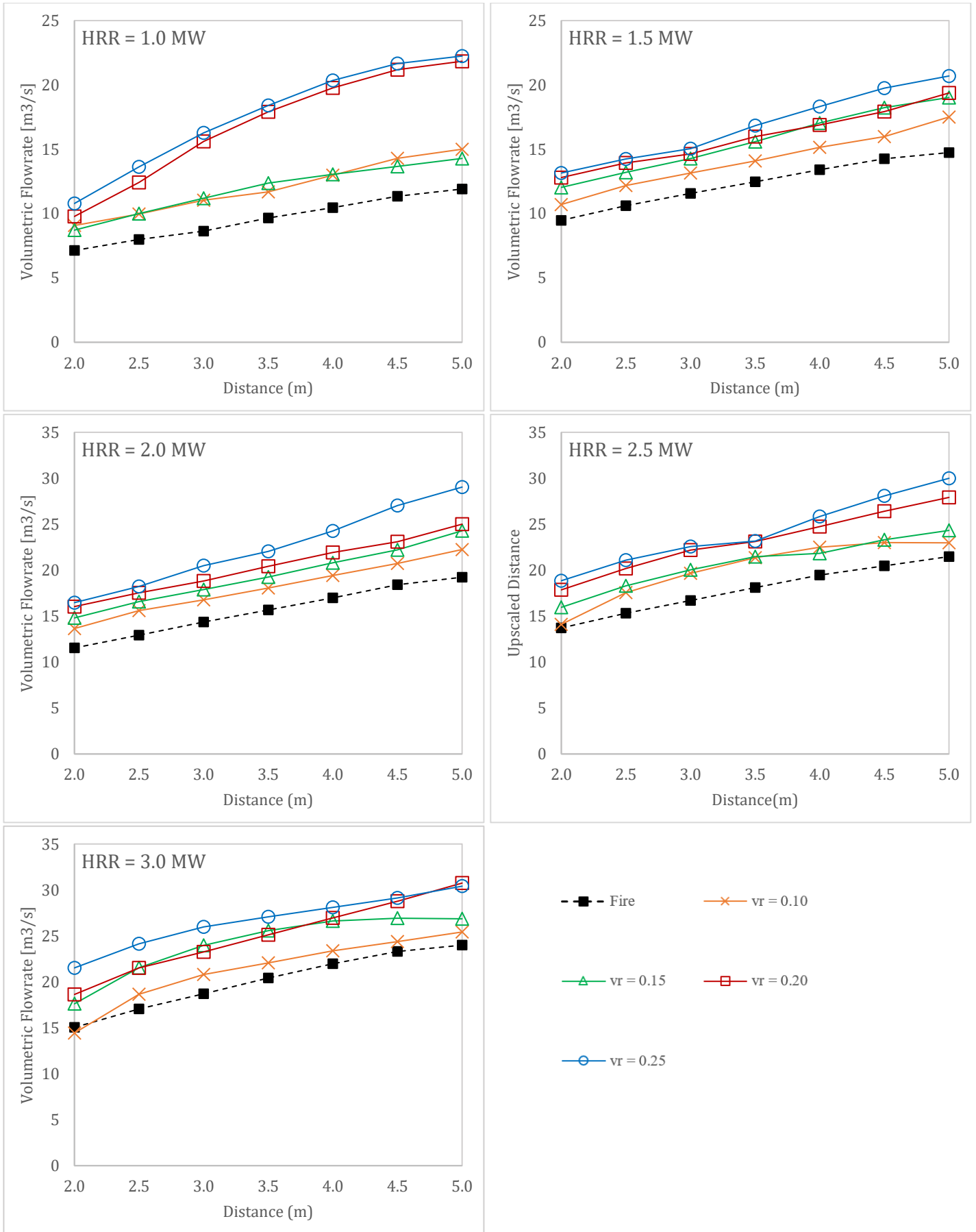Figure 17: Average excess temperature for full-scale FDS models

Figure 18: Volumetric Flowrate for full-scale FDS models

As it can be seen in these figures, the velocity ratio ($vr$) plays a significant role on the characteristics of the ceiling jet. This is due to the fact that the average plume temperature and velocity depend on the selection of $vr$, i.e., the radius of the plume for integration of the Gaussian profiles. Hence, a smaller $vr$ results in an integration over a larger radius, and consequently decreasing the average temperature and velocity of the fire plume. This leads to a lower ceiling jet temperature and velocity, as depicted in these figures.

Moreover, it was seen that no single value of $vr$ can provide accurate ceiling jet temperature across the full range of heat release rates. Instead, accurately predicted temperatures seem to shift toward cases with higher $vr$ value in larger fires as shown in Table 4, but this needs to be further examined to draw any generalized conclusion. In any case, considering the common heat release rates for office fires, the case with $vr = 0.15$ was selected for all subsequent small-scale simulations in order to eliminate the effect of $vr$ on the interpretation of small-scale results.

Table 4: Average deviations in full-scale ceiling jet temperature between hot air plume and fire simulations

| HRR | $vr = 0.1$ | $vr = 0.15$ | $vr = 0.2$ | $vr = 0.25$ |
|---|---|---|---|---|
| 1.0 $MW$ | 9 % | 7 % | 11 % | 36 % |
| 1.5 $MW$ | 25 % | 9 % | 21 % | 22 % |
| 2.0 $MW$ | 10 % | 11 % | 14 % | 32 % |
| 2.5 $MW$ | 13 % | 14 % | 9 % | 29 % |
| 3.0 $MW$ | 34 % | 16 % | 10 % | 3 % |

## Small-scale FDS Results

The previously discussed full-scale simulations with an actual fire and hot air flow were downscaled with scale factors of $1/10, 1/15$ and $1/20$. As mentioned above, small-scale simulations with the hot air model only considered $vr = 0.15$ so that the results only present the effects associated with the scale factor.

The average ceiling jet temperature and the upscaled volumetric flowrate are compared between the small-scale simulations with hot air plumes (with legend "Model") and actual fires (with legend "Fire") against the corresponding full-scale simulations with actual fire. Figure 19 shows an example for the full-scale $2.0\ MW$ fire, but the complete comparison charts can be found in the appendix.

In order to have a better overview of the accuracy of small-scale simulations using hot air plumes and actual fires in predicting the average ceiling jet temperature and its volumetric flowrate from full-scale simulations using actual fires, the ratios of small-scale to full-scale values were calculated. These comparisons are summarized in Figure 20 and Figure 21 for the average temperature and the volumetric flowrate, respectively.
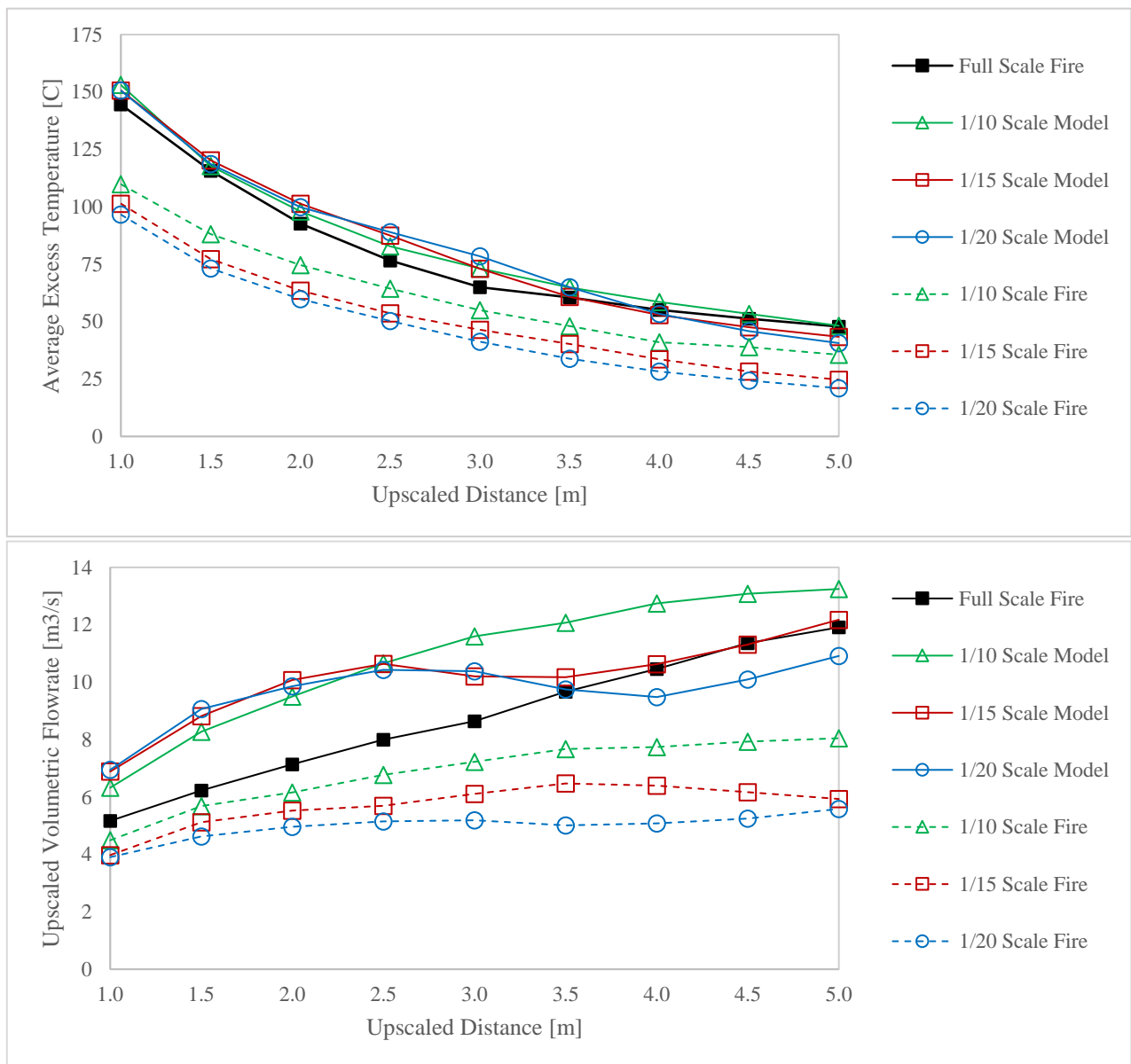


Figure 19: Comparison of small-scale models and small-scale fires and corresponding full-scale model
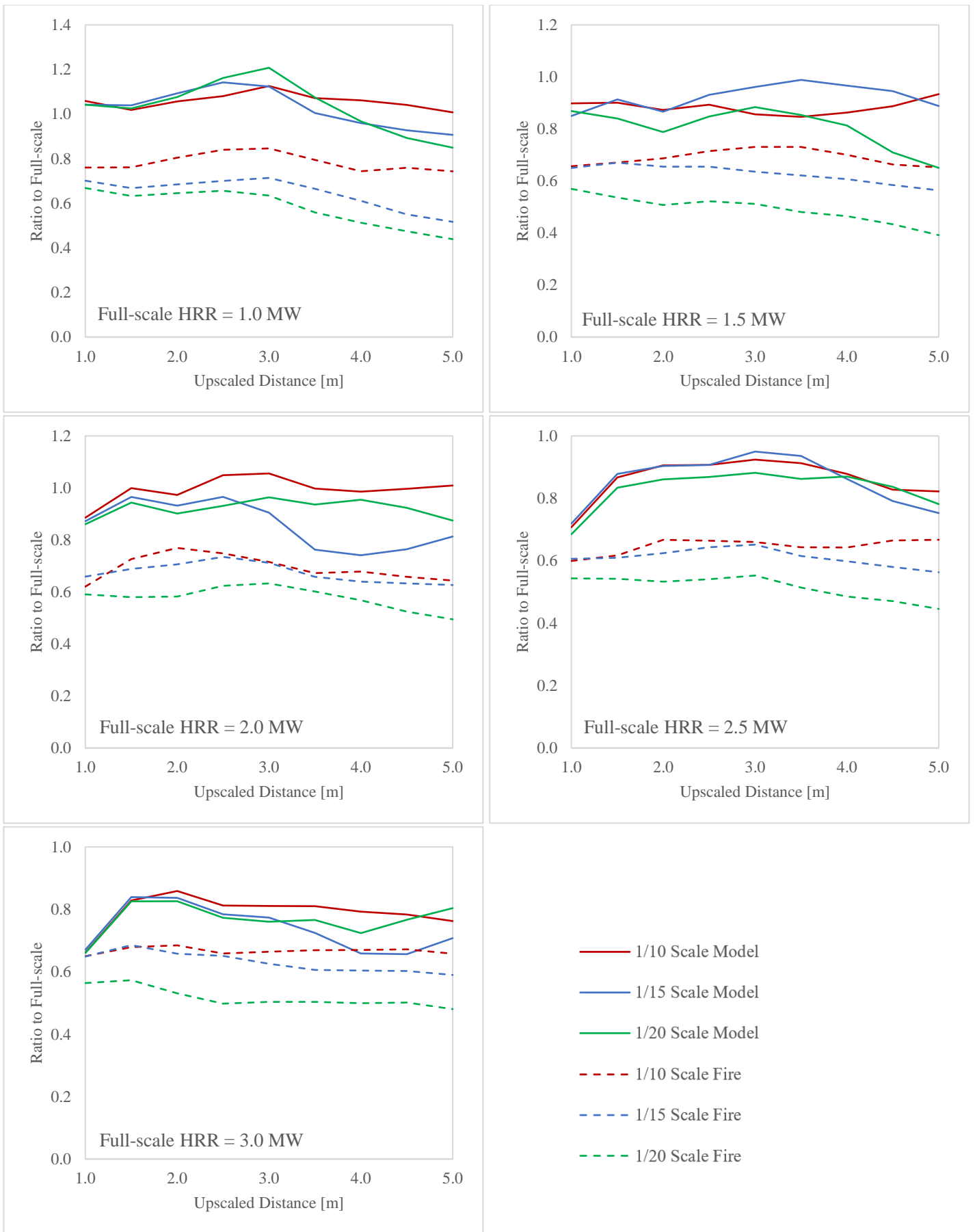
Figure 20: Ratio of small-scale to full-scale values for average excess temperature
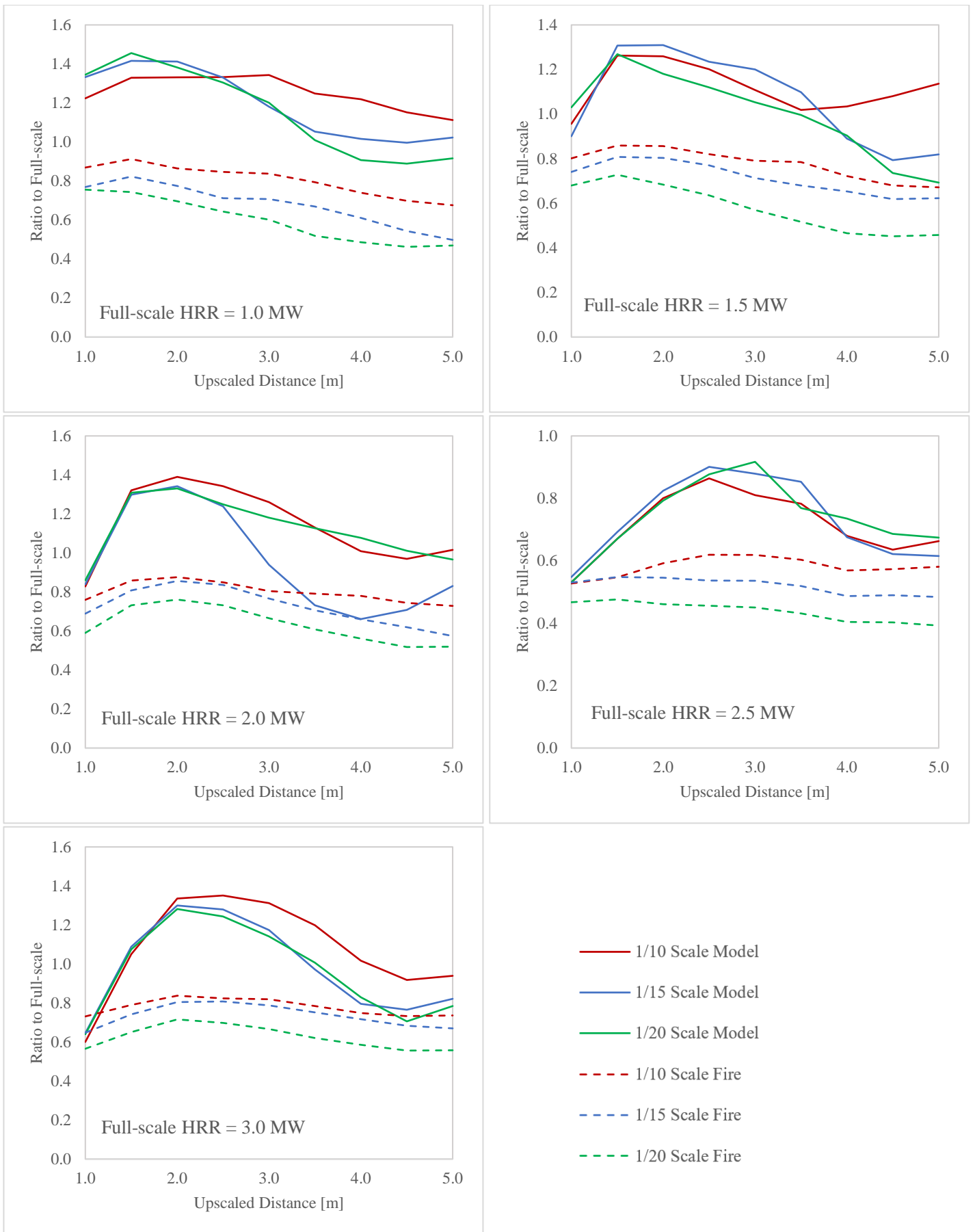
Figure 21: Ratio of small-scale to full-scale values for volumetric flowrate

A key finding from Figure 20 is the difference between small-scale simulations using hot air plumes with the proposed method and small-scale simulations using actual fires. It is evident that the average excess temperatures have smaller deviations for the proposed method in all fire sizes when compared against the full-scale fires. Thus, the ceiling jet can be better modelled with the hot air plume rather than the downscaled fire.

While the volumetric flowrates shown in Figure 21 are also better predicted for the proposed model (overall ratios are closer to 1), the trends are different for the proposed model by showing an initial overshoot followed by an undershoot in all heat release rates, especially for larger fires. This was assumed to be due to the inherently different flow patterns in the plume impingement region between a purely buoyant flow and a momentum-driven flow. This is shown in Figure 22 in the form of velocity contours for full-scale 3 *MW* fire simulation and small-scale simulations with hot air plumes. As the fire size increases, the entrance height is closer to the ceiling, thus the overshoot and undershoots are greater.
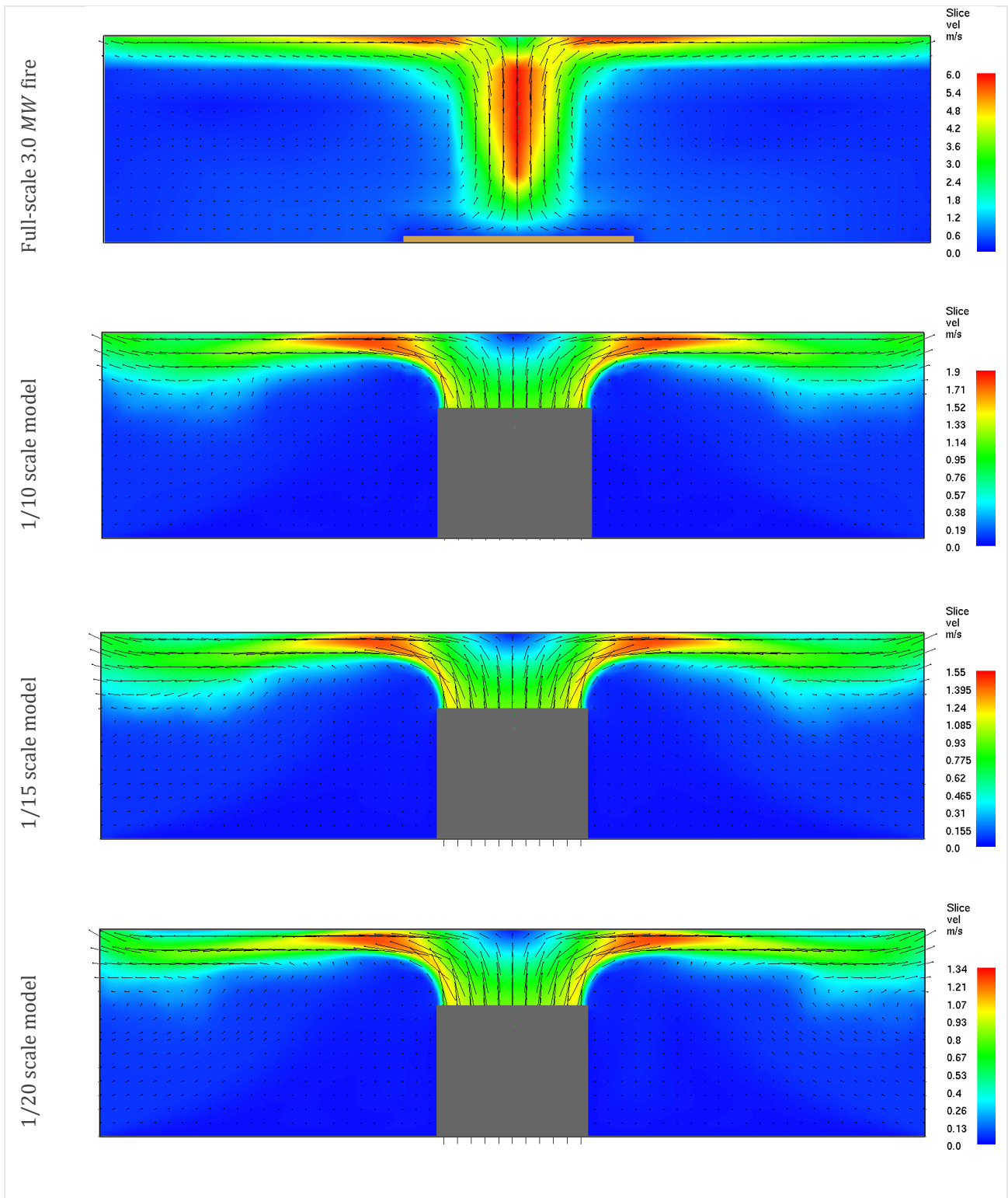
Figure 22: Comparison of velocity contours

# Experimental Results

Different scale factors were directly correlated with the ceiling height during experiments, i.e., the height of the columns. In order to measure the ceiling jet temperature, nine thermocouples were placed below the ceiling. Thermocouple junctions were fixed at a distance of $12\ mm$ from the ceiling board, thus the measurement data corresponded to the heights of $288\ mm$, $188\ mm$, and $138\ mm$ for 1/10, 1/15, and 1/20 scale factors, respectively, and when upscaling the measurement data, these readings corresponded to $2.88\ m$, $2.83\ mm$, and $2.78\ m$ for full-scale simulations. However, in order to be able to compare measurement results between different scale factors, the temperatures from simulations were averaged over $2.78 - 2.88\ m$ for all cases. Figure 23 to Figure 27 present these comparisons for different full-scale heat release rates, where the legends "Fire" and "Model" refer to the FDS simulations with actual fires and the proposed model with hot air plumes, respectively. It should be noted that no experiments were conducted for $2.0\ MW$, $2.5\ MW$, and $3.0\ MW$ fires in 1/10 scale factor due to the operation limitations of the experimental equipment.
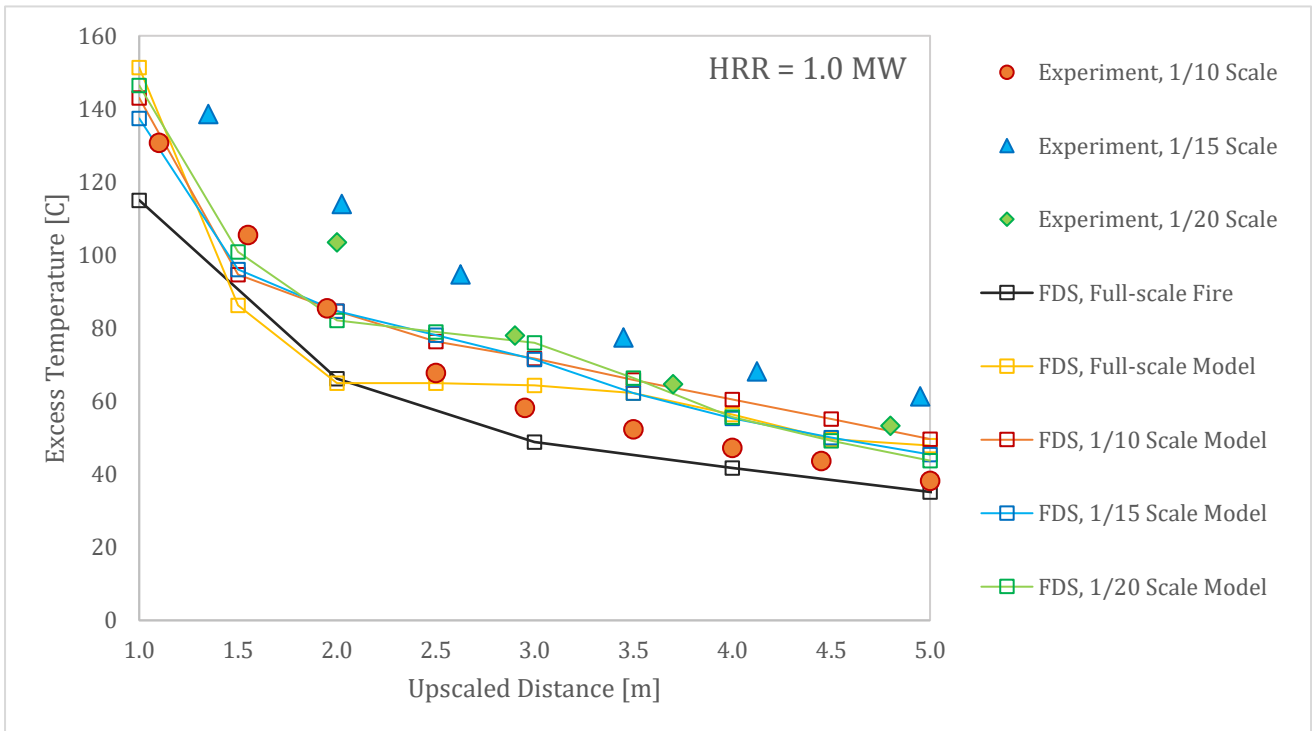


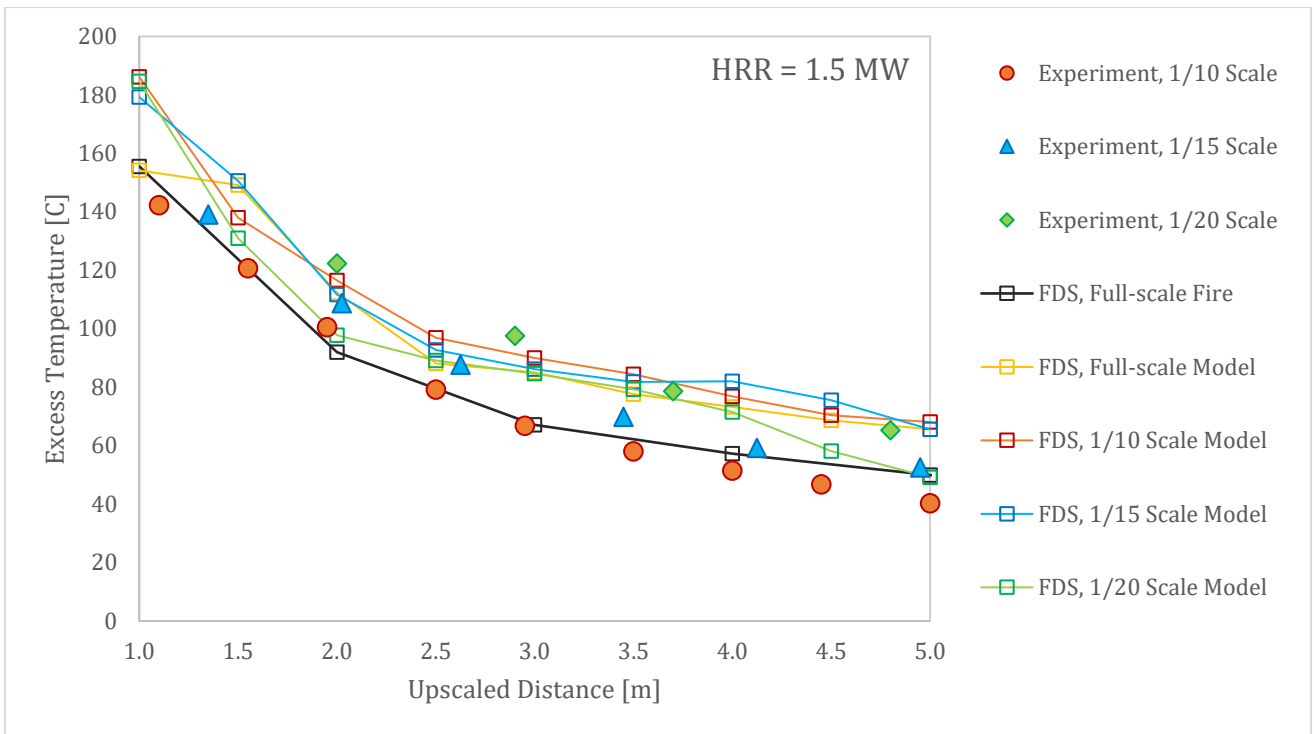Figure 23: Comparison between experimental and simulation results for 1.0 MW fire

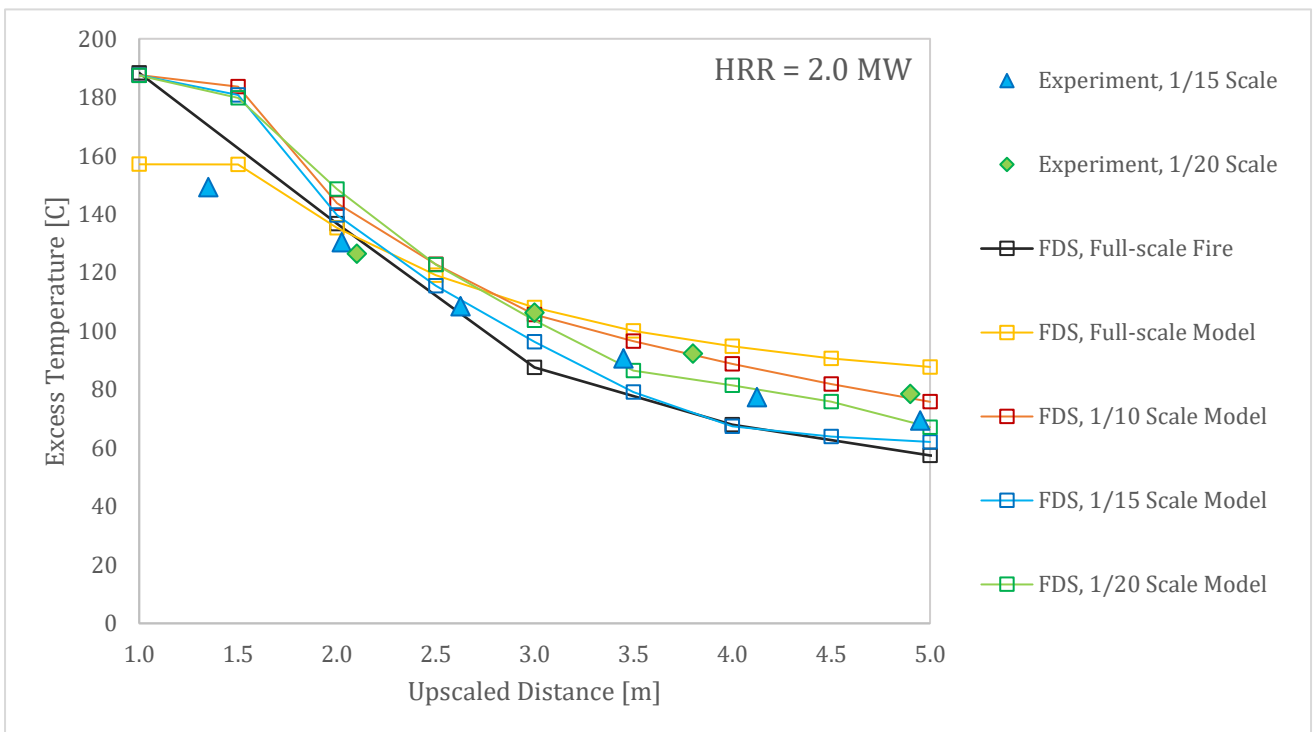Figure 24: Comparison between experimental and simulation results for 1.5 MW fire



Figure 25: Comparison between experimental and simulation results for 2.0 MW fire
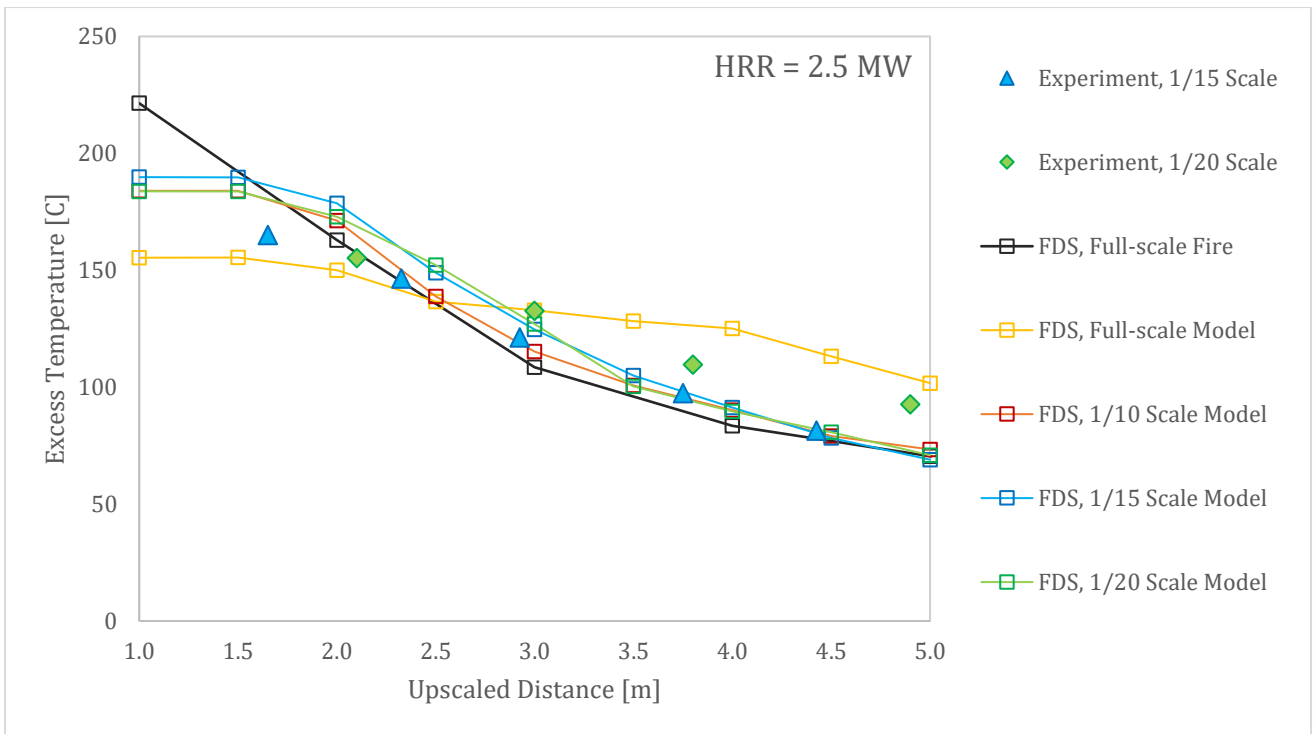
Figure 26: Comparison between experimental and simulation results for 2.5 MW fire
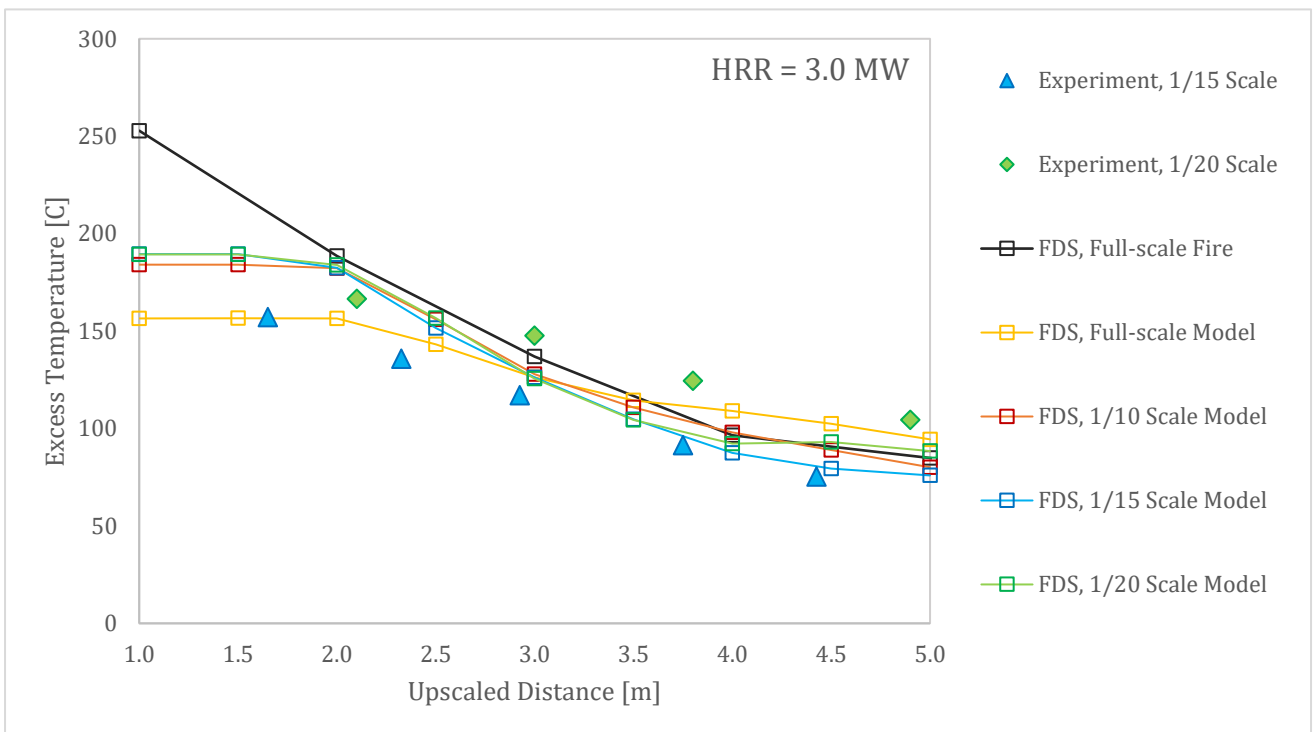


Figure 27: Comparison between experimental and simulation results for 3.0 MW fire

These figures show similar trends between the experimental results and FDS simulations both in full scale and small scales. There is a good agreement between small-scale simulations and the experimental data. For instance, the measured excess temperatures are higher than full-scale fire simulations at low heat release rates while for larger fires, the measured temperatures are slightly lower, which was also seen in Figure 20 for small-scale simulations. Figure 28 shows an overall view of all experimental results compared with full-scale simulations of actual fires.
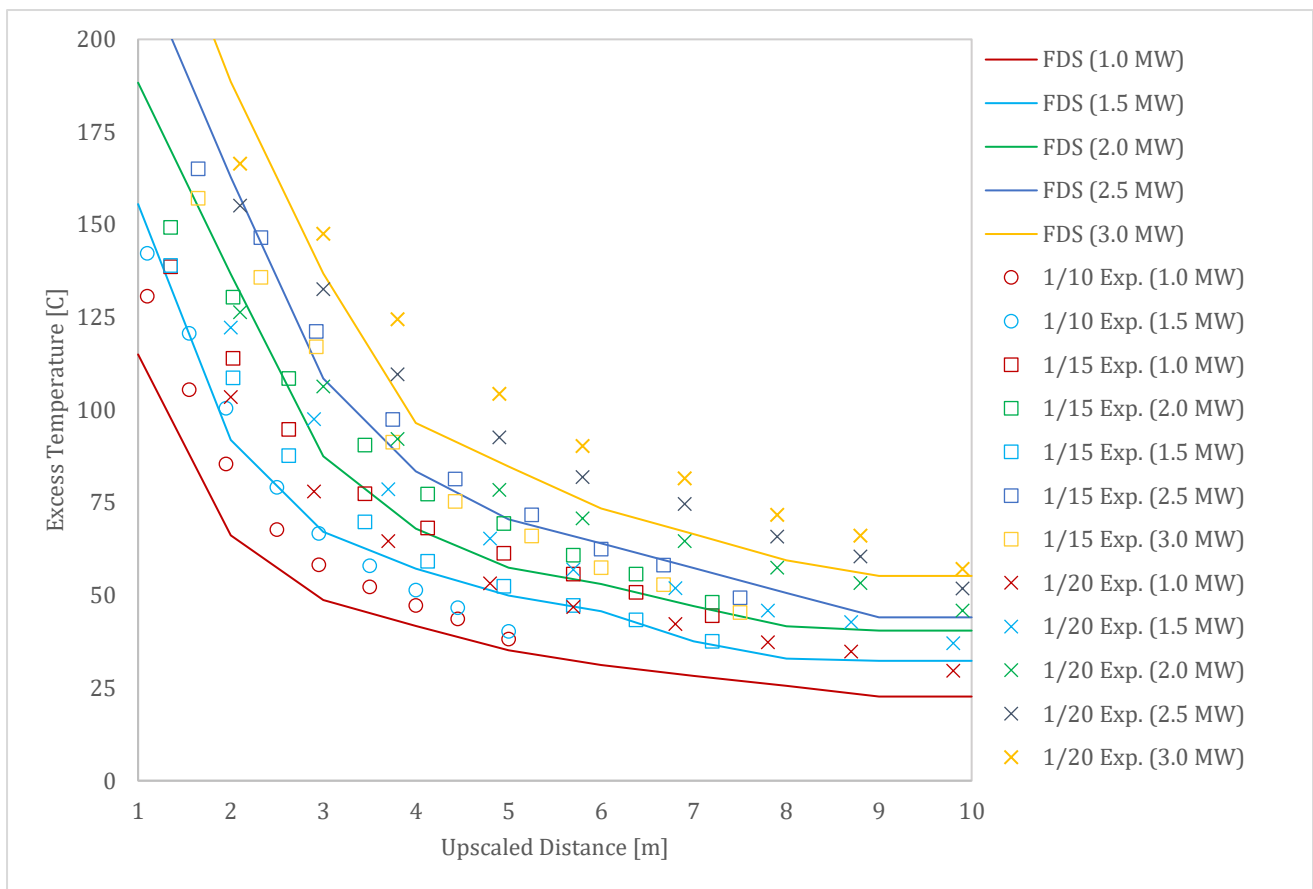


Figure 28: Overall comparison of experimental results with full-scale fire simulations

As it can be seen from this figure, the experimental results generally have good agreements with fire simulations. However, it should be noted that there are two discrepancies due to experimental error with the 1/15 scale tests: a) temperatures are lower for $3.0\ MW$ than $2.5\ MW$, b) temperatures are higher for $1.0\ MW$ than $1.5\ MW$. These were later seen to be due to the discrepancies in the adjusted volumetric flowrates during measurements for the $3.0\ MW$ and $1.0\ MW$ fires at 1/15 scale (for instance the ambient volumetric flowrate had dropped to $32.5\ m^3/hr$ during measurement recordings of $3\ MW$ fire test instead of being $35\ m^3/hr$).

## Experimental Uncertainty

Since the measurement tolerance of thermocouples was 0.1 ℃, the error bars for experimental data would be invisible in previous figures. However, in order to have an estimate of the experimental uncertainties and identify the factors with major impacts on the temperature measurements, one experiment was carried out in different days. In this regard, the pressure of the combustion chamber was significantly affected by the combustion, and consequently imposed fluctuating static pressure drops on the inlet fan. This was seen to impact the volumetric flowrate delivered by the fan, and lead to noticeable deviations in temperature measurements for the ceiling jet. As an example, Figure 29 compares the average measurement readings per minute in two different days with 2.5 $MW$ fire at 1/15 scale. Note that the hot air entrance temperature was similar in both tests while the ambient volumetric flowrate of the fan differed by less than 5 $m^3/hr$ between the two tests. Temperature measurements for these two tests differed from 1 ℃ up to 12 ℃ at different locations, which to great extents were due to the different flowrates, as the measurement differences for each day had significantly less fluctuations.
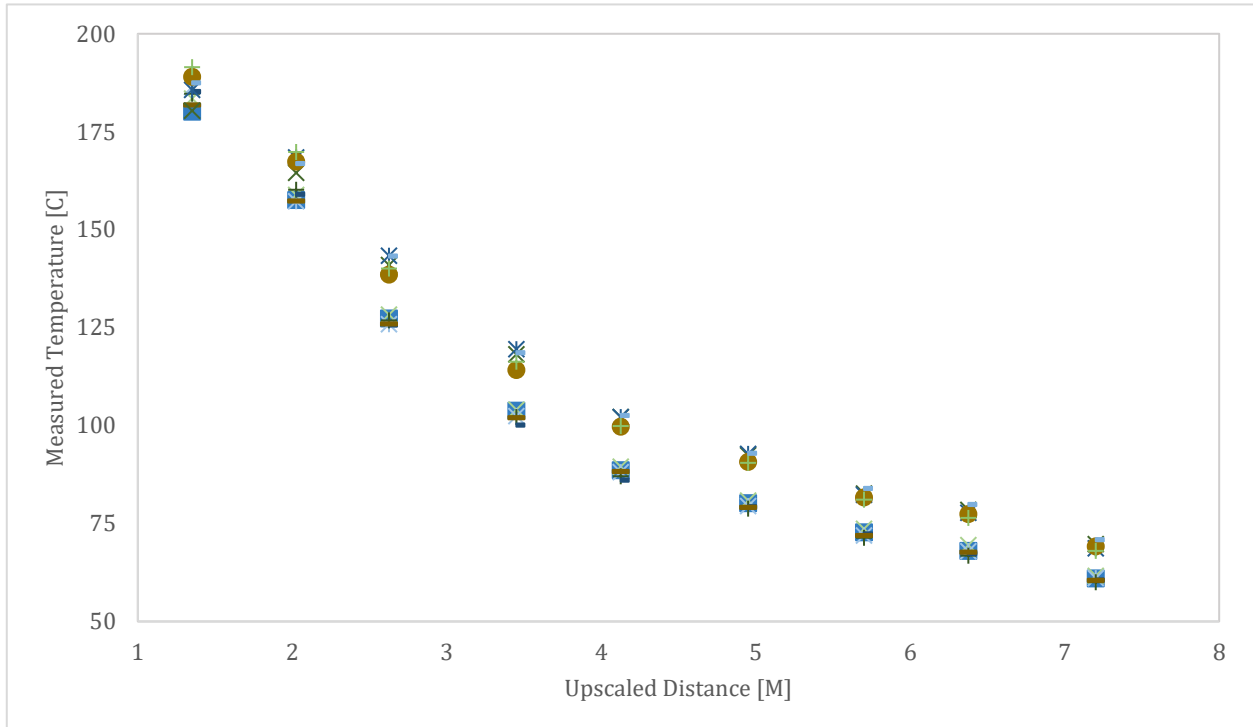


Figure 29: ceiling jet temperature readings during two separate tests for one experiment

# 4. Discussion

In this chapter, the accuracy of the hot air plume model using the proposed method is evaluated by comparing the present experimental and simulation results with existing empirical correlations for the ceiling jet temperature that are widely accepted and applied.

For the case of ceiling jet temperatures, empirical correlations by Alpert for weak plumes and the correlations by Heskestad and Hamada for strong plumes are widely appreciated. The correlation by Heskestad and Hamada is based on experimental measurements of the ceiling jet temperature with propane with the heat release rates of $12 - 764\ kW$ [25]. The correlation is known to be accurate for strong plumes where the free flame height is smaller than twice the ceiling height, and since this covers all scenarios in the present thesis, it can serve as an appropriate tool to validate the experimental results. Moreover, the full-scale experiments by Heskestad and Hamada were based on burning propane, which is the same fuel for the present experiments. This correlation is reported in [25] with different notation:

$$\Delta T/\Delta T_0 \ = \ 1.92(r/b)^{-1} - \exp[1.61(1 - r/b)] \qquad\qquad \text{(Eq. 16)}$$

Where $r$ represents the distance from the plume centerline and $\Delta T_0$ represents the excess temperature in the plume centerline at the height of the ceiling for an open fire. For the present study, this excess temperature is calculated from (Eq. 1). In addition, $b$ represents the radius at which the excess temperature equals half the value at the centerline and is given by [25]:

$$b \ = \ 0.42 \left[ \left( c_p \rho_\infty \right)^{4/5} T_\infty^{3/5}\ g^{2/5} \right]^{-1/2} \frac{T_0^{1/2}\ \dot{Q}_c^{2/5}}{\Delta T_0^{3/5}} \qquad\qquad \text{(Eq. 17)}$$

For the case of weak plumes where the mean flame height is much smaller than the ceiling height, the correlations by Alpert provide accurate predictions of ceiling jet excess temperature and velocity (although ratio of the heights is not quantitatively specified in [25]). The earlier version of these correlations were updated based on more recent experimental results and accounting for the convective heat release rate instead of the total heat release rate, and the equation for the excess temperature takes the form [25]:

$$\Delta T = 6.721 \frac{\dot{Q}_c^{2/3}}{(H-z_0)^{5/3}} \left(\frac{r}{H-z_0}\right)^{-0.6545} \qquad \text{(Eq. 18)}$$

It should be noted that (Eq. 16) and (Eq. 18) are reported to be valid in the range $b < r < 40b$, and $r > 0.134\,(H-z_0)$ which are both respected in all measurement locations in the present experiments. Considering an ambient temperature of $20\,°\text{C}$ which was approximately the case during all tests, the ceiling jet excess temperature was calculated using these equations for the heat release rates studied in the present thesis. Small-scale experimental results and full-scale simulation results are compared against these two correlations in Figure 30 to Figure 34 corresponding to full-scale heat release rates from $1.0\,MW$ to $3.0\,MW$.
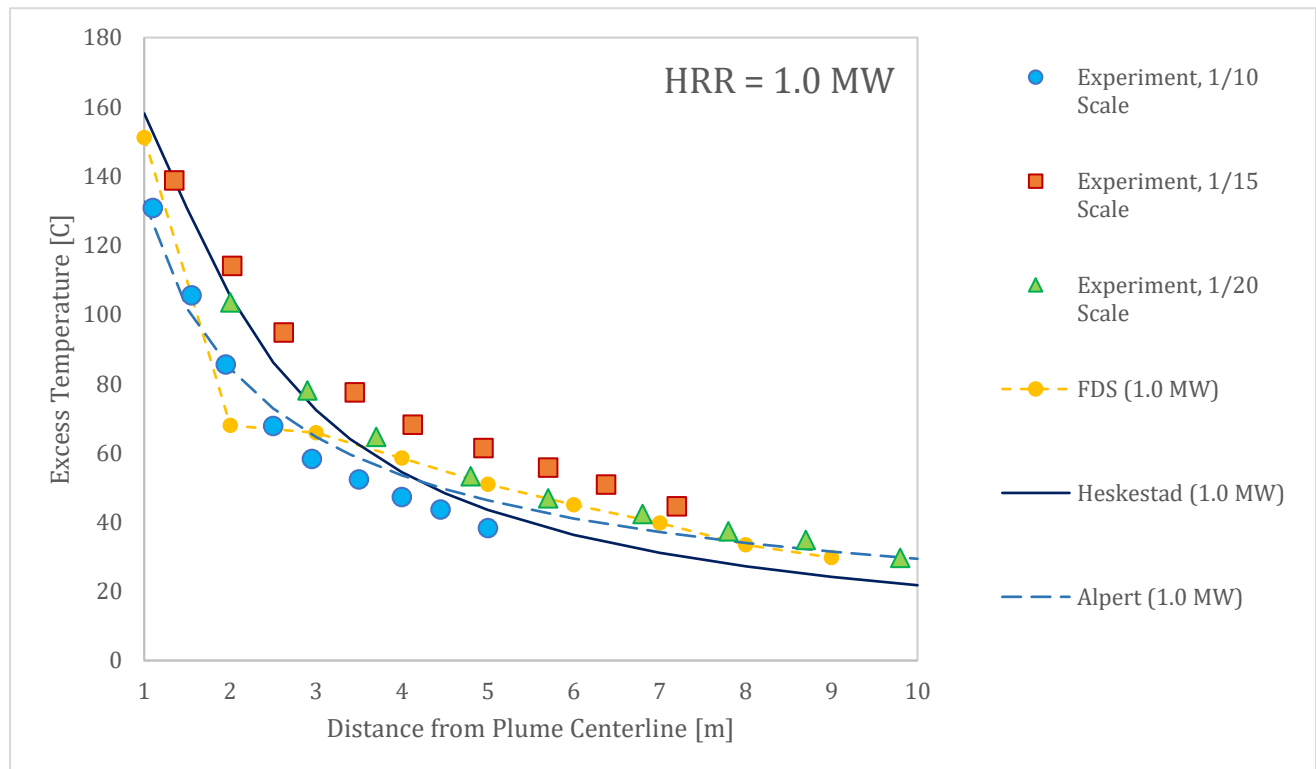


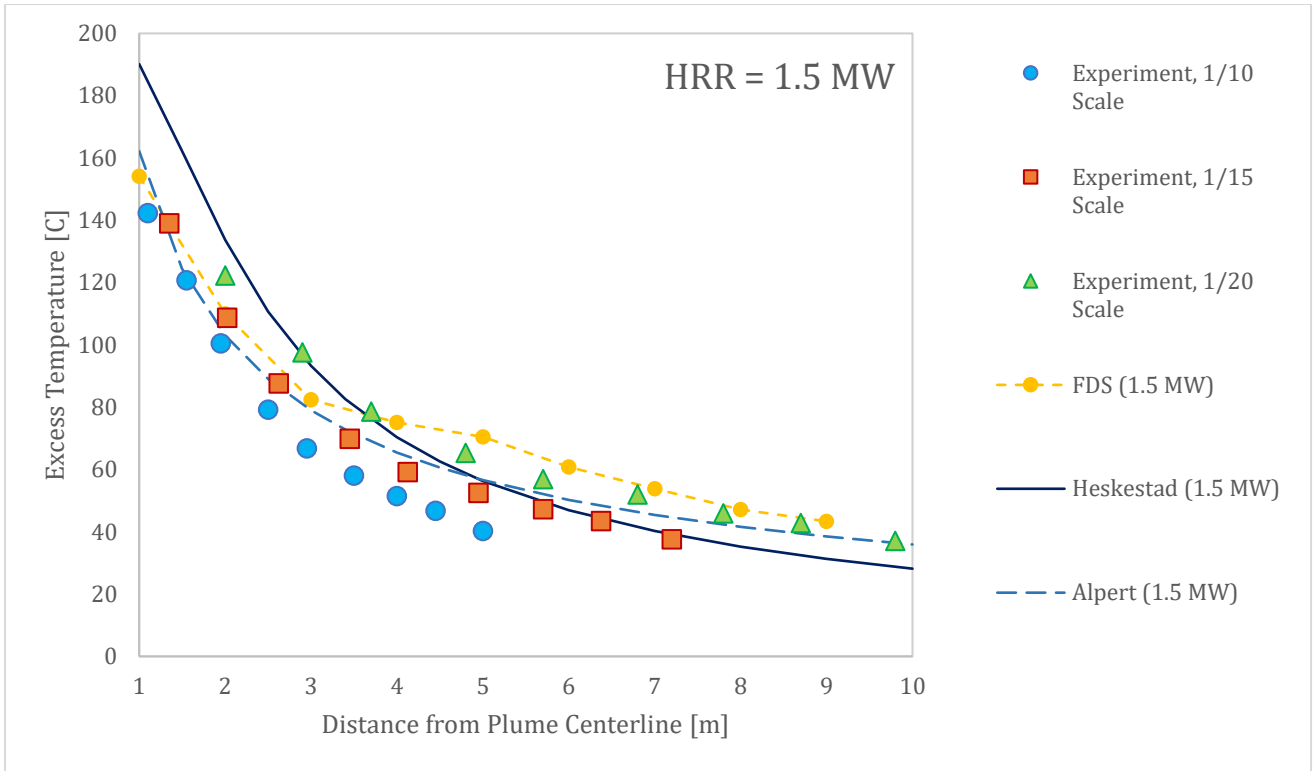Figure 30: Comparison of present results with literature for 1 $MW$ fire

Figure 31: Comparison of present results with literature for 1.5 *MW* fire
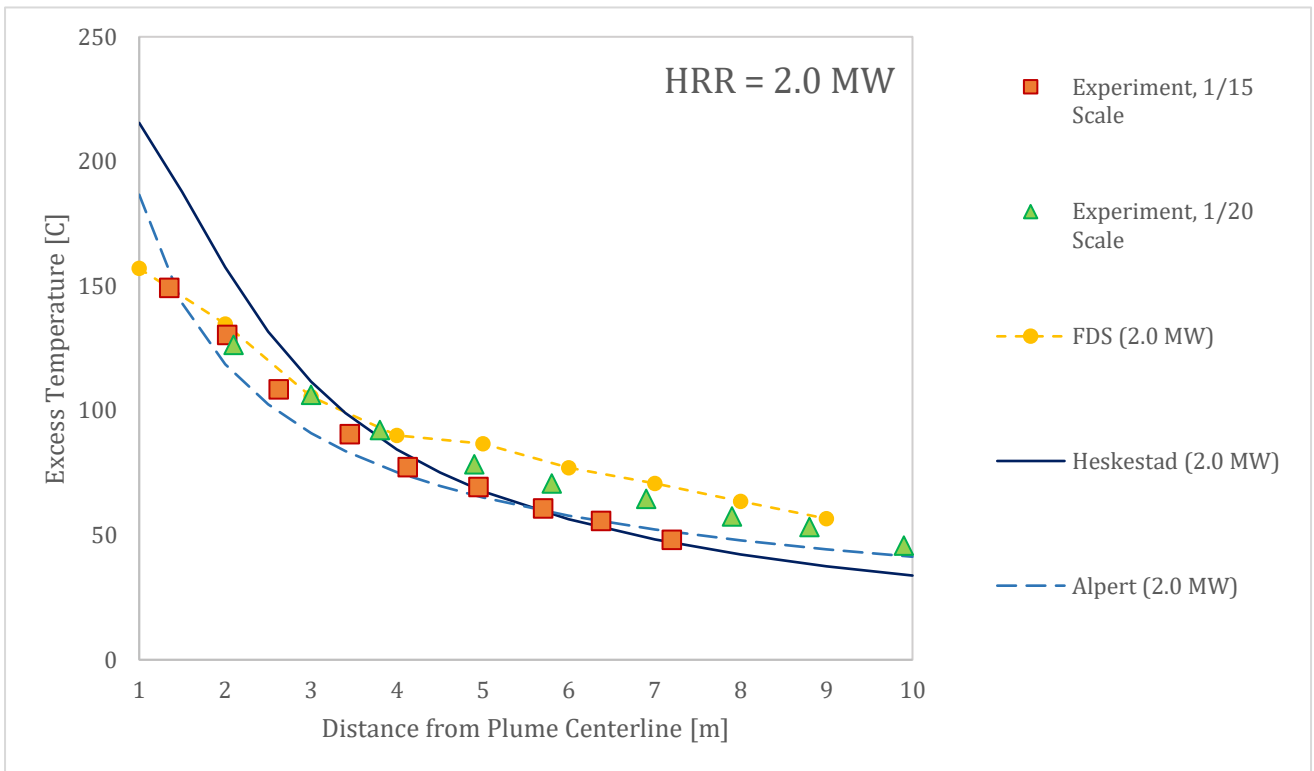


Figure 32: Comparison of present results with literature for 2 *MW* fire
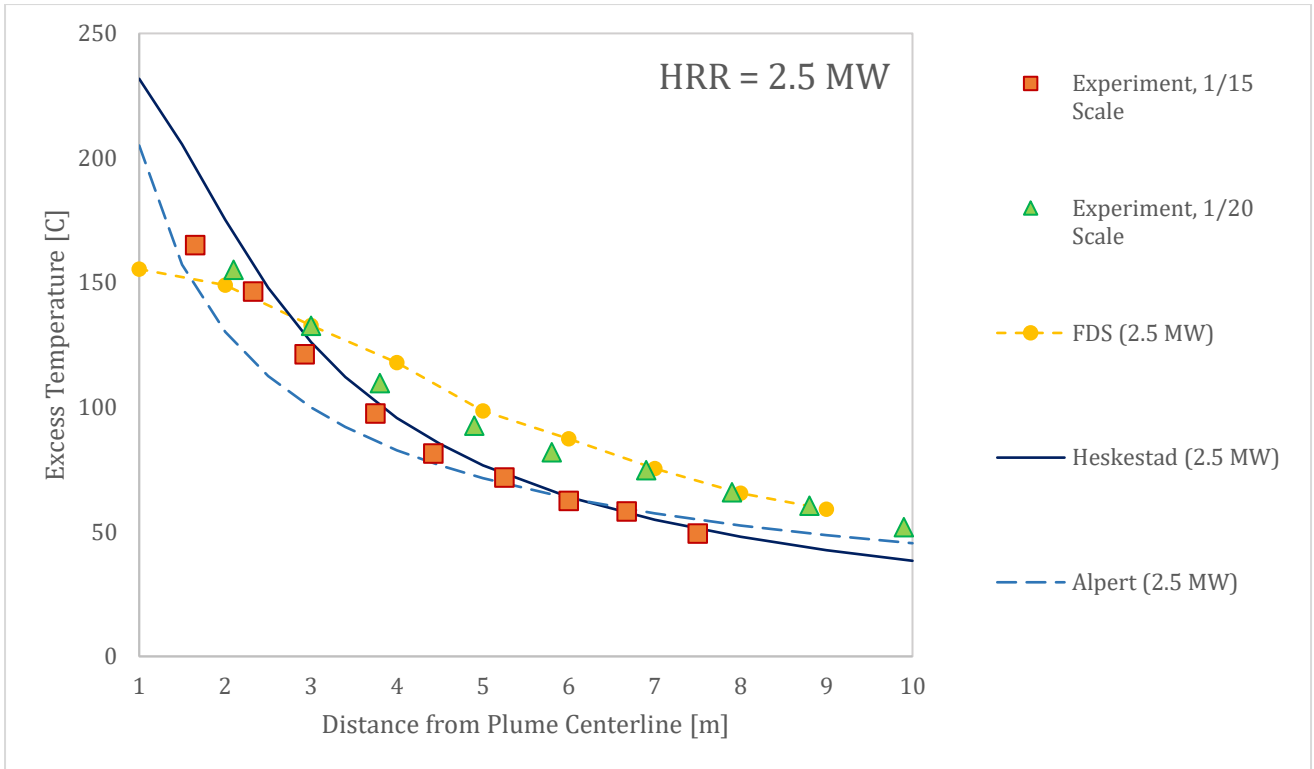
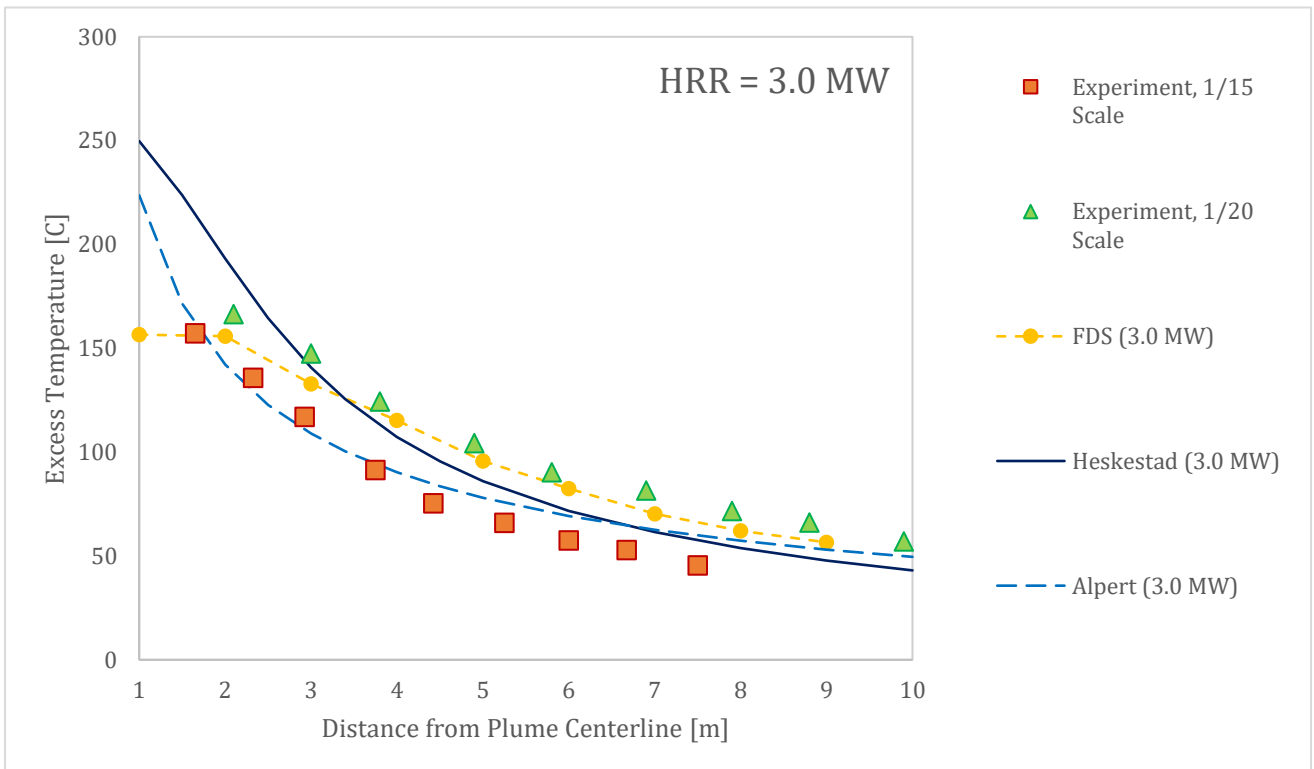Figure 33: Comparison of present results with literature for 2.5 *MW* fire



Figure 34: Comparison of present results with literature for 3 *MW* fire

These figures suggest acceptably similar trends between the experimental and simulation data with the hot air plume using the proposed method and the predictions based on empirical correlations of Heskestad and Hamada and Alpert. The average deviations of the present results from the correlation of Heskestad and Hamada are summarized in Table 5.

Table 5: Average deviation of present results from the correlation by Heskestad and Hamada

| | Full-scale HRR ($MW$) | Average deviation over all measurements in: | | | |
|---|---|---|---|---|---|
| | | Full-scale | 1/10 Scale | 1/15 Scale | 1/20 Scale |
| Experiments | 1 | - | 16 % | 29 % | 21 % |
| | 1.5 | - | 27 % | 11 % | 17 % |
| | 2 | - | - | 9 % | 22 % |
| | 2.5 | - | - | 5 % | 23 % |
| | 3 | - | - | 21 % | 22 % |
| Simulations | 1 | 14 % | 13 % | 9 % | 9 % |
| | 1.5 | 12 % | 10 % | 12 % | 11 % |
| | 2 | 15 % | 7 % | 13 % | 6 % |
| | 2.5 | 22 % | 8 % | 6 % | 7 % |
| | 3 | 15 % | 11 % | 14 % | 10 % |

These deviations are generally improved with the hot air plume model when compared against the small-scale simulation results using downscaled fires. These results show that it could be feasible to overcome the issue of weak turbulence in small-scale studies related to the ceiling jet temperature. In other words, the proposed method can be capable of extending the limits of downscaling in building geometries for those studies where the effects particularly associated with flames and smoke plume region are less relevant than the ceiling jet formation and its temperature at further distances downstream the fire source. While a minimum ceiling height of 30 $cm$ is recommended in the literature to ensure that the plume would be sufficiently turbulent (such as [18] reported in [17]), the present experiments were conducted with the ceiling heights up to half this value.

Based on the findings of the present thesis, replacing the fire source with an appropriate momentum-driven jet can provide a reliable substitute for large-scale fire tests, especially with the purpose of validating simulation results. Experimentation with a larger scale reduction factor is considerably more economical in terms of equipment costs, thus the proposed method could be more accessible for some engineering applications for validation or demonstration purposes. For instance, when the flames are replaced with the hot air plume at approximately 200 °C, building the set-up would be considerably less expensive, as there are lower requirements for high-temperature resistance of construction material.

It should be noted that the present thesis served as the first step in evaluating the feasibility of the proposed method in small-scale experiments for studying the smoke and heat control, hence a simple geometry was selected to allow for better comparison against existing empirical correlations. The applicability of such method in more complex geometries, including an enclosed compartment or a compartment with non-flat ceiling, as well as in scenarios combined with a smoke and heat extraction system requires further investigations. On the other hand, further examinations are useful in distinguishing the sources of deviations and improving the accuracy of the results. For instance, the round plume of hot air was replaced with a rectangular duct for practical reasons in the experiments and subsequent simulations. This is clearly a simplification of the geometry and might account for a portion of the error with respect to the considered empirical correlations, especially since the entrance height of the hot air plume was not sufficiently far from the ceiling to allow for development of the flow fields before the plume impinges on the ceiling.

# 5. Conclusions

A new method was proposed in the present thesis for small-scale testing in building spaces where the focus is on characterizing the ceiling jet such as studies involving ducted smoke and heat control systems. The proposed method draws an analogy between the fire-induced smoke and a hot air plume by replacing the purely buoyant smoke plume with a combined momentum and buoyancy driven flow. The analogy was based on preserving the momentum and energy of the smoke plume from an actual fire and ensuring that similar values are contained within the flow of hot air.

Empirical correlations were used to estimate these quantities based on integration of the Gaussian profiles from the smoke plume velocity and temperature and Heskestad's correlations for centerline values as well as the entrainment rate. Since office buildings were selected as the case study for the present thesis, the design fire ranged from $1\ MW$ to $3\ MW$ with a heat release rate per unit area of approximately $260\ kW/m^2$. Hence, the mean flame heights ranged from $1.5\ m$ to $1.9\ m$ while the ceiling height was selected as $3\ m$ for all trials.

As the radius of the smoke plume has a significant impact on its average temperature and velocity derived by integration, different FDS simulations were designed to determine an appropriate plume radius for which the ceiling jet characteristics were sufficiently accurate compared to the ceiling jet from an actual fire. The integration radius was translated into a dimensionless parameter, velocity ratio ($vr$) defined as the ratio of the plume velocity at distance $R$ to the centerline velocity, which was defined based on the smoke plume velocity profile. Following a preliminary analysis, 20 full-scale simulations were conducted for the heat release rates and mentioned above and velocity ratios from $0.10$ to $0.25$.

Using a single value for the velocity ratio ($vr = 15$), small-scale simulations were carried out for the same heat release rates using Froude scaling and geometric scale factors of 1/10, 1/15, and 1/20. Comparisons were made in terms of the ceiling jet temperature and volumetric flowrates between the full-scale simulations with a fire

source, small-scale simulations with downscaled fires, and small-scale simulations with the hot air plume. In addition, 13 small-scale experiments were conducted with the hot air plume corresponding to full-scale heat release rates of $1\ MW$, $1.5\ MW$, $2\ MW$, $2.5\ MW$, and $3\ MW$ with 1/10, 1/15, and 1/20 scale factors. Lastly, the ceiling jet temperatures were compared between the present experimental and simulation results and empirical correlations by Heskestad and Hamada and by Alpert, derived from full-scale experiments.

Comparisons between full-scale simulations with the proposed model and the corresponding fires showed that the optimum velocity ratio depends on the size of the fire. In this regard, smaller $vr$ values resulted in more accurate ceiling jet temperature predictions for lower heat release rates, but the simulations with larger velocity ratios could better replicate the actual ceiling jet of larger fires.

An interesting outcome from small-scale analyses was the improvement in replicating the ceiling jet characteristics of full-scale fires with the proposed method compared to simply downscaling the actual fire. While the ceiling jet temperatures were still slightly underestimated for small-scale simulations with the hot air plume, the predictions were considerably more accurate than small-scale simulations with downscaled fires. This was related to the initial momentum of the hot air which can partially compensate for the weak turbulence of a purely buoyant plume in small-scales, which is known to be the primary obstacle when downscaling models with low ceiling heights.

In addition, the volumetric flowrates were generally less underestimated with the proposed model in small scales. However, due to the intrinsic differences in flow patterns and velocity fields between a purely buoyant plume and a momentum-driven flow, the ratio of small-scale to full-scale flowrates showed an initial overshoot (approximately 20%) at short distances from the plume impingement region.

The experimental results for the ceiling jet temperatures were in good agreement with the simulations, and the overall deviation of measurement data from the widely appreciated correlations for ceiling jet temperature were within an acceptable range, especially when considering the simplifications that were made when designing experiments based on the proposed method, such as replacing the circular entrance duct for hot air with a rectangular duct due to practical considerations.

The present thesis served as the first step in evaluating the feasibility of conducting small-scale studies for building models with greater scale reduction factors than normally applicable for downscaled actual fires. Although there was an agreement between the experimental and simulation measurements based on the proposed method and predictions based on empirical correlations derived from full-scale experiments in the literature, the applicability of such method for more complex fire scenarios requires further investigation. In this regard, future research on evaluating the feasibility of such method in more complex scenarios can provide valuable outcomes. These scenarios include but are not limited to:

- Experiments in other building geometries, such as corridors and enclosed compartments.

- Evaluating the accuracy of the hot air plume model in combination with smoke and heat control systems, i.e., the effects associated with smoke extraction ducts, extraction rates, duct opening orientation, etc.

- Feasibility studies for transient compartment fires, e.g., comparing the predicted smoke layer descent time using the proposed method against the values derived from fire-induced smoke.

# Acknowledgements

# References

[1]     Y. Alarie, Toxicity of fire smoke, Crit. Rev. Toxicol. 32 (2002) 259–289.

[2]     J.H. Klote, Smoke control, in: SFPE Handb. Fire Prot. Eng., Springer, 2016: pp. 1785–1823.

[3]     N. Traina, S. Kerber, D.C. Kyritsis, G.P. Horn, Occupant Tenability in Single Family Homes: Part I—Impact of Structure Type, Fire Location and Interior Doors Prior to Fire Department Arrival, Fire Technol. 53 (2017) 1589–1610. https://doi.org/10.1007/s10694-017-0651-5.

[4]     R.K. Janardhan, S. Hostikka, Experiments and numerical simulations of pressure effects in apartment fires, Fire Technol. 53 (2017) 1353–1377.

[5]     W. Węgrzyński, Transient characteristic of the flow of heat and mass in a fire as the basis for optimized solution for smoke exhaust, Int. J. Heat Mass Transf. 114 (2017) 483–500.

[6]     D. Hopkin, C. Hopkin, M. Spearpoint, B. Ralph, R. Van Coile, Scoping study on the significance of mesh resolution vs. Scenario uncertainty in the CFD modelling of residential smoke control systems, in: Interflam 2019, 2019.

[7]     N. Tilley, P. Rauwoens, D. Fauconnier, B. Merci, On the extrapolation of CFD results for smoke and heat control in reduced-scale set-ups to full scale: Atrium configuration, Fire Saf. J. 59 (2013) 160–165.

[8]     J.G. Quintiere, Fundamentals of fire phenomena, (2006).

[9]     J.G. Quintiere, Scaling applications in fire research, Fire Saf. J. 15 (1989) 3–29.

[10]    J. Quintiere, B.J. McCaffrey, T. Kashiwagi, A scaling study of a corridor subject to a room fire, Combust. Sci. Technol. 18 (1978) 1–19.

[11]    H. Ingason, Y.Z. Li, Model scale tunnel fire tests with longitudinal ventilation, Fire Saf. J. 45 (2010) 371–384.

[12]    H. Ingason, Y.Z. Li, Model scale tunnel fire tests with point extraction ventilation, J. Fire Prot. Eng. 21 (2011) 5–36.

[13]    X. Jiang, M. Liu, J. Wang, Y. Li, Study on induced airflow velocity of point smoke extraction in road tunnel fires, Tunn. Undergr. Sp. Technol. 71 (2018) 637–643.

[14]    I. Horváth, J. van Beeck, B. Merci, Full-scale and reduced-scale tests on smoke movement in case of car park fire, Fire Saf. J. 57 (2013) 35–43.

[15]    K.D. Steckler, H.R. Baum, J.G. Quintiere, Salt water modeling of fire induced flows in multicompartment enclosures, in: Symp. Combust., Elsevier, 1988: pp. 143–149.

[16]    G. Maragkos, P. Rauwoens, B. Merci, Application of FDS and FireFOAM in large eddy simulations of a turbulent buoyant helium plume, Combust. Sci. Technol. 184 (2012) 1108–1120.

[17]    M. Zimny, P. Antosiewicz, G. Krajewski, T. Burdzy, A. Krasuski, W. Węgrzyński, Several Problems with Froude-Number Based Scale Modeling of Fires in Small Compartments, Energies. 12 (2019) 3625.

[18]    J.G. Quintiere, A.C. Carey, L. Reeves, L.K. McCarthy, Scale modeling in fire reconstruction, National Criminal Justice Reference Service, Office of Justice Programs, 2017.

[19]    D. Arini, F. Pancawardani, M.A. Santoso, B. Sugiarto, Y.S. Nugroho, Froude modelling of fire phenomena: observation of fire-induced smoke movement in basement structure for firefighting purpose, Procedia Eng. 170 (2017) 182–188.

[20]    M.M. Barsim, M.A. Bassily, H.M. El-Batsh, Y.A. Rihan, M.M. Sherif, Froude scaling modeling in an Atrium Fire equipped with natural and transient forced ventilation, Int. J. Vent. 19 (2020) 201–223.

[21]    B.R. Morton, G.I. Taylor, J.S. Turner, Turbulent gravitational convection from maintained and instantaneous sources, Proc. R. Soc. London. Ser. A. Math. Phys. Sci. 234 (1956) 1–23.

[22]    O. Vauquelin, G. Michaux, C. Lucchesi, Scaling laws for a buoyant release used to simulate fire-induced smoke in laboratory experiments, Fire Saf. J. 44 (2009) 665–667.

[23]    O. Vauquelin, Experimental simulations of fire-induced smoke control in tunnels using an "air–helium reduced scale model": Principle, limitations, results and future, Tunn. Undergr. Sp. Technol. 23 (2008) 171–178.

[24]    G. Zhao, L. Wang, Using helium smoke as a surrogate of fire smoke for the study of atrium smoke filling, J. Fire Sci. 32 (2014) 431–447.

[25]    R.L. Alpert, Ceiling Jet FLows, in: M.J. Hurley, D.T. Gottuk, J.R. Hall Jr, K. Harada, E.D. Kuligowski, M. Puchovsky, J.M. Watts Jr, C.J. WIECZOREK (Eds.), SFPE Handb. Fire Prot. Eng., Springer, 2015: pp. 429–454.

[26]    Gunnar Heskestad, Fire Plumes, Flame Height, and Air Entrainment, in: M.J. Hurley, D.T. Gottuk, J.R. Hall Jr, K. Harada, E.D. Kuligowski, M. Puchovsky, J.M. Watts Jr, C.J. WIECZOREK (Eds.), SFPE Handb. Fire Prot. Eng., Springer, 2015: pp. 396–428.

[27]    W. Węgrzyński, P. Antosiewicz, T. Burdzy, M. Zimny, A. Krasuski, Smoke obscuration measurements in reduced-scale fire modelling based on Froude number similarity, Sensors. 19 (2019) 3628.

[28]    S. Kakegawa, Y. Yahshiro, H. Satoh, H. Kurioka, I. Kasahara, Y. Ikehata, N. Saito, T. Turuda, Design fires for means of egress in office buildings based on full-scale fire experiments, Fire Saf. Sci. 7 (2003) 975–986.

[29]    S.B. Pope, S.B. Pope, Turbulent flows, Cambridge university press, 2000.

[30]    K. McGrattan, S. Hostikka, R. McDermott, J. Floyd, C. Weinschenk, K. Overholt, Fire dynamics simulator user's guide, NIST Spec. Publ. 1019 (2013) 1–339.

[31]    N. Johansson, J. Wahlqvist, P. Van Hees, Simple ceiling jet correlation derived from numerical experiments, in: Int. Interflam Conf. Interflam 2013, Interscience Communications Ltd, 2013: pp. 61–72.

# Appendix

Comparison between small-scale to full-scale ratios of maximum excess temperature, average temperature, and volumetric flowrate between the proposed model with the hot air plume and normally downscaled fire models are shown here for $1\ MW$, $1.5\ MW$, $2\ MW$, $2.5\ MW$, and $3\ MW$ fires in full scales, respectively.